An amino-terminal threonine/serine motif is necessary for activity of the Crp/Fnr homolog, MrpC, and for *Myxococcus xanthus* developmental robustness

Brooke E. Feeley[1], Vidhi Bhardwaj[2†], Maeve McLaughlin[1], Stephen Diggs[3], Gregor M. Blaha[3], and Penelope I. Higgs[1*]

[1] Department of Biological Sciences, Wayne State University, Detroit, MI, USA

[2] Department of Ecophysiology, Max Planck Institute for Terrestrial Microbiology, Marburg, Hesse, Germany

[3] Department of Biochemistry, University of California, Riverside, Riverside, CA, USA

Running title: MrpC TTSS amino terminal motif

Key words: *Myxococcus xanthus,* MrpC, Crp/Fnr, development, biofilm, developmental buffer

* Corresponding author

E-Mail: pihiggs@wayne.edu (PIH)

Ph: (313) 577-9241

†present address: Innoplexus AG, Frankfurt, Germany, D-65760

Summary

The Crp/Fnr family of transcriptional regulators play central roles in transcriptional control of diverse physiological responses. Activation of individual family members is controlled by a surprising diversity of mechanisms tuned to the particular physiological responses or lifestyles that they regulate. MrpC is a Crp/Fnr homolog that plays an essential role in controlling the *Myxococcus xanthus* developmental program. A long-standing model proposed that MrpC activity is controlled by the Pkn8/Pkn14 serine/threonine kinase cascade which phosphorylates MrpC on threonine residue(s) located in its extreme amino terminus. In this study, we demonstrate that a stretch of consecutive threonine and serine residues, T_{21} T_{22} S_{23} $S_{24,}$ is necessary for MrpC activity by promoting efficient DNA binding. Mass spectrometry analysis indicated the TTSS motif is not directly phosphorylated by Pkn14 *in vitro* but is necessary for efficient Pkn14-dependent phosphorylation on several residues in the remainder of the protein. Pkn8 and Pkn14 kinase activities do not play obvious roles in controlling MrpC activity in wild type *M. xanthus* under laboratory conditions, but likely modulate MrpC DNA binding in response to unknown environmental conditions. Interestingly, mutational analysis of the TTSS motif caused non-robust developmental phenotypes, revealing that MrpC plays a role in developmental buffering.

INTRODUCTION

Crp/Fnr transcriptional regulators belong to a large family characterized by an amino terminal cyclic nucleotide binding ("cNMP") domain followed by a characteristic DNA binding domain comprised of a helix-turn-helix motif (Korner *et al.*, 2003, Soberon-Chavez *et al.*, 2017). These transcriptional regulators have been shown to control several processes central to the lifestyle of their respective bacteria, such as carbon or nitrogen source utilization, aerobic/anaerobic transition, developmental processes, and pathogenicity (Lazazzera *et al.*, 1993, Spiro & Guest, 1990, Derouaux *et al.*, 2004, Kanack *et al.*, 2006). Despite the presence of a common cNMP domain, individual groups within the family are regulated by diverse signals and transcriptional activity is controlled by different mechanisms. For example, the canonical *E. coli* Crp protein controls catabolite repression. Crp exists as an inactive dimer, which upon binding of cAMP results in allosteric reorientation of the DNA binding region allowing efficient binding to target DNA sequences (Saha *et al.*, 2015), where it activates or represses downstream genes by making specific (Benoff *et al.*, 2002). In contrast, for *E. coli* Fnr which induces genes necessary for anaerobic growth, activation is controlled by monomer to dimer transition (Lazazzera *et al.*, 1993). Fnr senses oxygen via an associated Fe-S cofactor coordinated by four cysteine residues. In the absence of oxygen (activating conditions), the Fnr dimer is stabilized by a 4Fe-4S cluster and can bind to target sequences to activate or repress gene expression (Kiley & Beinert, 1998). In the presence of oxygen, the cluster transitions ultimately to an 2Fe-2S cluster leading to destabilization of the dimer and loss of DNA binding. In yet another variation, the *Xanthomonas campestris* CLP protein, which controls several genes involved in

pathogenesis of plants, is a dimer which intrinsically binds target DNA sequences in the absence of ligand, but binding of di-c-GMP causes it to shift to an inactive conformation to release DNA binding sequences (Chin *et al.*, 2010).

MrpC is a Crp/Fnr family member necessary for the starvation-induced multicellular developmental program of *Myxococcus xanthus* (Sun & Shi, 2001). *M. xanthus* is a gram negative deltaproteobacterium commonly found in the soil (Munoz-Dorado *et al.*, 2016). In vegetative (non-developing conditions), *M. xanthus* is a cooperative predator. Swarms of *M. xanthus* cells glide in search of prey microorganisms or decaying organic material. Upon encountering prey, the swarm collectively releases antibiotics and degradative enzymes to paralyze and digest the prey. Upon nutrient poor conditions, the swarm enters a developmental program culminating in the formation of multicellular fruiting bodies filled with environmentally resistant spores. During this program, cells are first directed to move into haystack-shaped mounds (aggregation centers) of approximately 100,000 cells. Exclusively within these mounds, cells are induced to differentiate into spores, forming mature fruiting bodies. Production of spores inside fruiting bodies is not the only cell fate and accounts for only ~15% of the starting population (as determined for the *M. xanthus* strain DZ2 induced to develop under submerged culture)(Lee *et al.*, 2012). The majority of the cells (~80%) undergo cell lysis, likely via programmed cell death (Rosenbluh *et al.*, 1989, Wireman & Dworkin, 1977, Lee *et al.*, 2012). The remaining ~5% of cells are found as peripheral rods that remain outside of the fruiting bodies in a persister-like state (O'Connor & Zusman, 1991). Spore-filled fruiting bodies are quiescent and resistant to environmental insults,

such as desiccation and UV, but upon return of nutrients, spores can germinate *en mass* to produce a productive feeding swarm (Munoz-Dorado *et al.*, 2016).

MrpC plays a central role in the genetic regulatory network controlling the developmental program (Kroos, 2007), and an Δ*mrpC* mutant is incapable of aggregation and fails to launch the core sporulation program (Sun & Shi, 2001, McLaughlin *et al.*, 2018). The *mrpC* gene is upregulated early after starvation and is dependent upon the MrpAB two component signal transduction system (Sun & Shi, 2001). MrpB is an enhancer binding protein, which when activated by phosphorylation of its associated receiver domain, induces transcription of *mrpC* from a putative sigma^{54}-dependent promoter (Sun & Shi, 2001). Once produced, MrpC functions as a negative autoregulator, by competing with MrpB for overlapping binding sites in the *mrpC* promoter (McLaughlin *et al.*, 2018). At least two other MrpC binding sites located upstream of the *mrpC* transcriptional start, also contribute to negative autoregulation [(McLaughlin *et al.*, 2018) and unpublished data)].

MrpC is a global regulator, controlling at least 200 genes during the developmental program (Robinson *et al.*, 2014). A key downstream target is the transcription factor, FruA (Ueki & Inouye, 2003, Ogawa *et al.*, 1996). FruA is an orphan response regulator that is thought to induce aggregation and then sporulation in response to C-signaling, a cell-cell contact signal which increases in intensity as cells enter into aggregation centers (Saha *et al.*, 2019, Ellehauge *et al.*, 1998, Sogaard-Andersen & Kaiser, 1996). Activated FruA and MrpC act separately and in combination to regulate a number of genes necessary for differentiation of cells inside aggregation centers into spores (Son

et al., 2011, Lee *et al.*, 2011, Mittal & Kroos, 2009a, Mittal & Kroos, 2009b, Viswanathan *et al.*, 2007).

It is unclear how MrpC binding to target promoters is controlled. No native ligand for MrpC is currently known, and the protein binds efficiently to target promoters *in vitro* (Ueki & Inouye, 2003, Nariya & Inouye, 2006, Mittal & Kroos, 2009a, McLaughlin *et al.*, 2018) suggesting that MrpC is intrinsically able to binding target sequences in the absence of ligand. *In vivo*, MrpC is subject to several post-translational regulatory mechanisms. The EspAC signaling system functions early during development to activate an unknown protease to target MrpC to ensure only a gradual accumulation of MrpC that is presumably necessary for production of large, well-formed aggregation centers before the onset of sporulation (Schramm *et al.*, 2012, Higgs *et al.*, 2008, Cho & Zusman, 1999). In a second, apparently unrelated system, addition of nutrients to developing cells triggers unknown protease(s) to rapidly degrade MrpC allowing reversal out of the developmental program (prior to commitment to sporulation)(Rajagopalan & Kroos, 2014). Another post-translational regulation mechanism involves the serine/threonine protein kinase (STPK) cascade comprised of Pkn8 and Pkn14. *In vitro*, Pkn8 phosphorylates Pkn14, and Pkn14 phosphorylates MrpC on threonine residue(s) in its extreme amino terminus (Nariya & Inouye, 2005b, Inouye & Nariya, 2008, Nariya & Inouye, 2006). Phosphorylation was proposed to prevent LonD protease-dependent processing to remove the amino terminal 25 residues, producing 'MrpC2' (here termed $MrpC_{\Delta N25}$), a more active isoform. We have recently demonstrated, however, that MrpC's amino terminal extension is essential for

function *in vivo*, and that 'MrpC2' is likely an artifact of cell lysis (McLaughlin *et al.*, 2018).

To reconcile the previous connection between phosphorylation of the MrpC amino-terminus with the recent demonstration that the amino terminus is essential for function, we set out to revisit Pkn14-dependent phosphorylation of MrpC. We demonstrate here that a specific cluster of threonines and serines (termed the TTSS motif) in the amino-terminal region is essential for MrpC activity *in vivo*. Alanine substitution of the complete MrpC TTSS motif prevents efficient development by interfering in MrpC's negative autoregulation, proteolytic turnover, and transcriptional activation of FruA. Interestingly, while no single residue was necessary for activity, specific combinatorial substitutions within the TTSS motif produced highly variable developmental phenotypes revealing a previously unknown role for MrpC in developmental buffering. Mass spectrometry analysis of *in vitro* Pkn14-dependent phosphorylation of MrpC revealed that the MrpC TTSS motif is not directly phosphorylated by Pkn14 but is required for efficient phosphorylation of to several residues within the cNMP and DNA binding domains. Reexamination of the role of Pkn8/14 suggests they are not active kinases during the developmental program of wild type *M. xanthus* under laboratory conditions, but likely fine tune MrpC activity in response to unknown environmental conditions. Thus, our data revises the model for Pkn8/14 control over MrpC activity and identifies an unusual TTSS motif that likely plays a role in stabilizing transitions between active and inactive MrpC states.

RESULTS

A TTSS motif within the N-terminal extension is necessary for MrpC activity.

MrpC is a Crp/Fnr family transcriptional regulator with a 29 residue N-terminal extension that is essential for *in vivo* function (McLaughlin *et al.*, 2018). No activating ligand is known for MrpC, but it was previously reported that MrpC activity is regulated by a STPK cascade which was proposed to phosphorylate MrpC on threonine residue(s) within the first 25 residues (Nariya & Inouye, 2005b, Nariya & Inouye, 2006). Sequence analysis of the amino-terminal region of MrpC shows that there are only two threonine residues (at positions 21 and 22) which are directly followed by two consecutive serine residues (Fig. 1A). As serine and threonine residues can both be phosphorylated by Ser/Thr kinases, we considered the TTSS residues a putative phosphorylation motif. To examine whether this motif was important for activity, we generated a strain in which the TTSS residues were entirely substituted with alanines in the endogenous *mrpC* locus (*mrpC*$_{AAAA}$) and analyzed the resulting developmental phenotype under submerged culture conditions compared to the wild type and Δ*mrpC* strains. As expected, the wild type strain produced obvious aggregates between 34 and 48 hours which darkened by 72 hours of development, while the Δ*mrpC* strain failed to aggregate at all (Fig. 1B). The *mrpC*$_{AAAA}$ strain produced abnormally shallow and elongated aggregation streams that failed to progress to aggregation centers. Analysis of heat and sonication resistant spores at 72 hours of development indicated the wild type produced $2.6 \pm 0.5 \times 10^7$ heat and sonication resistant spores per well, while the Δ*mrpC* and *mrpC*$_{AAAA}$ mutants produced ≤ 0.01 % and 11 ± 10 % of wild type spore levels, respectively (Fig. 1C). Since launch of the sporulation program is coupled to completion of aggregation, we

could not distinguish whether defective sporulation by the *mrpC$_{AAAA}$* mutant was because it failed to complete aggregation or whether MrpC$_{AAAA}$ specifically interfered in induction of the sporulation program. To distinguish between these two possibilities, we examined the sporulation efficiency of wild type, Δ*mrpC*, and *mrpC$_{AAAA}$* strains upon chemical induction of sporulation which bypasses the requirement for aggregation (Dworkin & Gibson, 1964). For this assay, vegetative broth cultures of wild type, Δ*mrpC*, or *mrpC$_{AAAA}$* cells were treated with 0.5 M glycerol for 24 hours and heat and sonication resistant spores were counted. We observed that the Δ*mrpC* and *mrpC$_{AAAA}$* strains produced ≤ 0.01 and 11 ± 3 % of wildtype spore levels, respectively (Fig. 1C), suggesting that MrpC$_{AAAA}$ was strongly reduced in triggering spore differentiation.

To determine whether the *mrpC$_{AAAA}$* defective developmental and sporulation phenotypes were simply explained by reduction in MrpC stability, we compared the levels of MrpC produced from the wild type, and *mrpC$_{AAAA}$* strains at 0, 12, 18, 24, and 36 hours of development by anti-MrpC immunoblot. As expected, wild type MrpC protein began to accumulate at 12 hours but was absent by 36 hours (Fig. 1D). The MrpC$_{AAAA}$ protein had ~ 2-fold increased accumulation relative to the parent strain at 12 hours but was also absent by 36 hours development (Fig 1D). Thus, the development defect observed in by the *mrpC$_{AAAA}$* mutant was not due to failure to accumulate MrpC$_{AAAA}$, strongly suggesting that an intact TTSS motif is necessary for MrpC function.

Consecutive intact residues within the MrpC TTSS motif are necessary for robust development

To determine whether substitution of any specific residue within the TTSS motif was sufficient to observe the *mrpC*$_{AAAA}$ phenotype, strains bearing individual alanine substitutions of each TTSS residue were generated in the endogenous *mrpC* locus. These strains, producing MrpC$_{T21A,}$ MrpC$_{T22A}$, MrpC$_{S23A}$ or MrpC$_{S24A}$ are hereafter designated with the TTSS substitution (i.e. *mrpC*$_{ATSS}$, *mrpC*$_{TASS}$, *mrpC*$_{TTAS}$ or *mrpC*$_{TTSA}$, respectively). These mutants produced developmental phenotypes and sporulation efficiencies similar to the wild type strain (Fig. S1), suggesting no one particular individual residue in the TTSS motif was necessary for activity. Furthermore, substitution of both threonines or both serines of the TTSS motif in the endogenous *mrpC* gene (strains *mrpC*$_{AASS}$ or *mrpC*$_{TTAA}$), respectively) also produced a wild type phenotype suggesting the neither of the threonine nor the serine residues were functionally redundant (Fig. S1).

We next considered whether any intact single residue within the TTSS motif was sufficient for function by constructing two different mutants in which only one residue was available for phosphorylation: *mrpC*$_{TAAA}$ or *mrpC*$_{AAAS}$. As these mutants proved difficult to generate in the endogenous *mrpC* locus, we instead expressed the *mrpC*$_{TTSS}$ (wt), *mrpC*$_{AAAA}$, *mrpC*$_{TAAA}$, or *mrpC*$_{AAAS}$ clones from their endogenous promoter inserted at the Mx8 phage attachment (*attB*) site in the Δ*mrpC* background (Δ*mrpC attB*::P$_{mrpC}$-*mrpC*$_{TTSS}$, etc.; termed *att*::*mrpC*$_{TTSS,}$ etc. for short). The *att*::*mrpC*$_{TTSS}$ (wt) clone complemented Δ*mrpC*, although aggregation onset was observed on average four hours earlier than the DZ2 parent (data not shown). The *att*::*mrpC*$_{AAAA}$ mutant phenocopied *mrpC*$_{AAAA}$ generated at the endogenous locus (Fig. 1 and Fig. 2). Strikingly however, independent clones and replicates of the same clones of the *att*::*mrpC*$_{TAAA}$ or

231 *att*::*mrpC*$_{AAAS}$ strains did not display stable developmental phenotypes. To quantify the
232 extent of phenotypic variation between replicates and between clones, we used a high-
233 throughput, high resolution development imaging technique to generate movies of
234 strains undergoing development (Glaser & Higgs, 2019). Stages of development were
235 recorded for each movie and displayed as heat maps versus the indicated ranges of
236 hours post-starvation (Fig. 2). In this assay, wild type *mrpC* clones displayed robust
237 developmental phenotypes, with onset of aggregation observed between 24-29.5 hours
238 post starvation, followed by initial aggregates (30-35.5 h), aggregates after
239 consolidation/dissolution (36-41.5 h), mature immobile aggregates (42-47.5 h) and
240 darkened fruiting bodies (≥ 48 h). The *att*::*mrpC*$_{AAAA}$ clones consistently failed to
241 develop properly (Fig. 2). However, for the *att*::*mrpC*$_{TAAA}$ or *att*::*mrpC*$_{AAAS}$ strains,
242 significantly different developmental patterns were observed both among clones and
243 between replicates of the same clone (Fig. 2). Developmental patterns observed ranged
244 from early or delayed development to failure to develop (Fig. 2). We observed the same
245 variability in phenotypes when the *mrpC* variants were instead integrated at a different
246 secondary site [termed 1.38kb (Garcia-Moreno *et al.*, 2010)] in the Δ*mrpC* background,
247 indicating that the variability was not due to placement at the *attB* site (Fig. S2). These
248 results suggested that induction of development had become stochastic, perhaps
249 because the equilibrium between active and inactive MrpC was perturbed.
250 Assuming the TTSS motif was indeed necessary for phosphorylation, we postulated that
251 since the *mrpC*$_{AASS}$ and *mrpC*$_{TTAA}$ mutants displayed stable wild type phenotypes (Fig.
252 S1), perhaps any two intact TTSS residues were necessary for MrpC function. To test
253 this hypothesis, we generated *att*::*mrpC*$_{TASA}$ clones and again observed that this mutant

produced variable developmental phenotypes both between clones and replicates of the same clone (Fig. 2). Together, these results suggested that at least two consecutively intact TTSS residues were necessary for MrpC function. However, from these data it was not fully clear whether the TTSS motif was directly phosphorylated or whether it served as an important polar motif necessary for stable conformational switching or protein-protein interactions.

Finally, as an alternate genetic approach, we attempted to generate phosphomimetic mutations in which substitution with glutamic acid may mimic a phosphorylated amino acid (Dissmeyer & Schnittger, 2011). For these analyses, we generated *att*::*mrpC*$_{ETSS}$, *att*::*mrpC*$_{EAAA}$, or *att*::*mrpC*$_{EEAA}$ clones to examine whether "forcing" at least one phosphorylation but leaving the remaining motif intact, or generating "constitutive single only" or "constitutive double" phosphorylation states, could reveal a phospho-code relating to function. Analysis of the developmental phenotype of these mutants indicated the ETSS substitution produced slightly variable, delayed to wild type aggregation phenotypes with fruiting bodies that sometimes failed to darken (Fig. 2), which usually indicates impaired sporulation. Both the *att*::*mrpC*$_{EAAA}$ and *att*::*mrpC*$_{EEAA}$ mutants were essentially inactive and phenocopied the *att*::*mrpC*$_{AAAA}$ phenotype (data not shown). These results suggested either that glutamic acid substitution did not act as a phosphomimetic or that the TTSS motif is not a phosphorylation target.

Pkn14 phosphorylates MrpC in vitro *on several residues in the cNMP and DNA-binding domains*

To determine whether we could recapitulate the observation that Pkn14 phosphorylates MrpC *in vitro* (Nariya & Inouye, 2005b), we overexpressed and purified Strep affinity tagged-Pkn14 and a kinase-dead version of the protein in which the conserved lysine at position 48 which is predicted to be necessary for ATP binding (Hanks, 2003) was substituted with asparagine (Strep-Pkn14$_{K48N}$). Strep-Pkn14 or Strep-Pkn14$_{K48N}$ was incubated for 30 minutes in the presence of ATP, resolved by SDS-PAGE, and the resulting gel was incubated in phosphoprotein stain. Autophosphorylated Strep-Pkn14 could be detected readily, while the signal on Pkn14$_{K48N}$ was significantly reduced (Fig. 3A); the remaining signal was likely due to non-specific fluorescence because the Pkn14$_{K48N}$ protein was completely inactive when incubated in the presence of [γ-^{32}P] ATP (data not shown). We next repeated these assays in the presence of purified hexa-histidine affinity tagged (His$_6$) -MrpC, -MrpC lacking the 25 amino terminal residues (His$_6$-MrpC$_{\Delta N25}$), His$_6$-MrpC$_{AAAA}$, or the non-specific protein Trx-His$_6$. Phosphorylation of the MrpC protein could be detected, which was reduced 1.7- and 4.0-fold on His$_6$-MrpC$_{\Delta N25}$ or His$_6$-MrpC$_{AAAA}$, respectively. Some signal was observed on the non-specific protein Trx-His$_6$ (Fig. 3A). Thus, we recapitulated the result that Pkn14 appears to phosphorylate MrpC and show that phosphorylation is reduced (but not absent) if the TTSS motif is removed.

We next extended these analyses to examine which residues in His$_6$-MrpC or His$_6$-MrpC$_{AAAA}$ might be phosphorylated by Strep-Pkn14 *in vitro* using mass spectrometry. For this approach, Strep-Pkn14 or Strep-Pkn14$_{K48N}$ were incubated with His$_6$-MrpC or His$_6$-MrpC$_{AAAA}$ using the *in vitro* phosphorylation reaction conditions. Reactions were quenched, trypsin digested, and phosphopeptides were captured on titanium dioxide

columns, separated by liquid chromatography and subjected to mass spectrometry. In the Pkn14/MrpC reaction, we captured 72 phosphopeptides. With strict selection criteria (minimum 5 peptides detected, 0.1% false discovery rate), Ser/Thr phosphoresidues detected corresponded to MrpC S_{55}, T_{56} (within the cNMP-binding domain), and T_{173}, T_{176}, T_{191}, and T_{197} (within the DNA binding domain)(Fig. 3B). These phosphorylated residues were observed in two independent replicates, although the number of phosphopeptides captured varied slightly. In the Pkn14/MrpC$_{AAAA}$ reaction, we observed only 20 phosphopeptides, but they corresponded to the same sites as the wild type with the exception of T_{176} and T_{191}. As expected, no phosphopeptides could be detected in the Pkn14$_{K48N}$/MrpC or Pkn14$_{K48N}$/MrpC$_{AAAA}$ reactions, indicating that all phosphopeptides observed in the wild type Pkn14 reactions were a result of Pkn14 specifically. Thus, the TTSS motif was not in fact phosphorylated by Pkn14 *in vitro* suggesting the reduction in phosphorylation on the MrpC$_{AAAA}$ was likely a result of inefficient recognition of MrpC as a substrate by Pkn14.

To rule out that the conformation of His$_6$-MrpC$_{AAAA}$ was drastically perturbed, we compared the circular dichroism (CD) spectra of His$_6$-MrpC and His$_6$-MrpC$_{AAAA}$ under ionic conditions similar to those used in our *in vitro* assays (Fig. 3C). The secondary structures of His$_6$-MrpC$_{AAAA}$ and His$_6$-MrpC were identical, with characteristic absorbance peaks at λ = 208 and 220 nm. Thus, substitution of the TTSS motif with alanines did not produce drastic changes in the secondary structure of MrpC. Together, these results suggested that the TTSS motif may instead be a MrpC recognition motif.

322 *The Pkn8/Pkn14 kinase cascade does not inactivate MrpC in the wild type strain under*
323 *laboratory conditions*
324
325 Regardless of whether the TTSS motif is directly phosphorylated by Pkn14 or is merely
326 a recognition motif that facilitates Pkn14-dependent phosphorylation of MrpC at different
327 sites, the observation that the *mrpC*$_{AAAA}$ mutant does not develop suggested that
328 phosphorylation of MrpC would serve as an activation signal, rather than the inactivation
329 signal originally proposed based on the early developmental phenotypes previously
330 observed for both *pkn14* and *pkn8* mutant strains in the non-wildtype *M. xanthus*
331 background strain, DZF1 (Nariya & Inouye, 2005b). As the DZF1 (aka DK101) strain is
332 defective in a social motility system (Wall *et al.*, 1999) which can often perturb
333 developmental phenotypes (Lee *et al.*, 2012, Boynton *et al.*, 2013), we next sought to
334 reexamine the developmental phenotypes of strains lacking the Pkn8/Pkn14 kinase
335 cascade in our wild type DZ2 *M. xanthus* background. We therefore generated in-frame
336 deletions of *pkn14* and *pkn8* and constructed point mutations predicted to render each
337 protein kinase-dead in the endogenous locus of each gene (strains Δ*pkn14*, Δ*pkn8*,
338 *pkn14*$_{K48N}$, *pkn8*$_{K116N}$, respectively). When these strains and the wild type were induced
339 to develop under submerged culture conditions, the wild type strain produced visible
340 aggregation centers between 28- and 35-hours post-starvation, and $2.7 \pm 0.7 \times 10^7$ heat
341 and sonication resistant spores at 120 hours (Fig. 4A). In contrast to previously
342 published results, the Δ*pkn14* strain showed delayed aggregation: visible aggregation
343 centers were detected between 35 and 48 hours, approximately 6 hours later than the
344 wild type. By 120 hours of development, the Δ*pkn14* mutant sporulated at wild type

efficiencies (102 ± 15 % of wild type)(Fig. 4A and B). When we generated our Δ*pkn14* in the DZF1 strain background and developed the strains on nutrient limited CF agar (DZF1 strains do not develop under submerged culture), we observed the same early developmental phenotype originally observed (Nariya & Inouye, 2005b), while the DZ2 Δ*pkn14* strain again exhibited a delayed developmental phenotype (Fig. S3). Thus, we concluded that the difference in developmental phenotypes was not the result of different Δ*pkn14* constructs or developmental conditions assayed, but rather due to strain background. We and others have previously observed that the DZF1 strain background yields different mutant phenotypes compared to the wild type strains DZ2 and DK1622 (Lee *et al.*, 2012, Boynton *et al.*, 2013). These results in the wild type background were consistent with a model in which Pkn14-dpendent phosphorylation could activate MrpC.

Surprisingly, however, analysis of the *pkn14*$_{K48N}$ mutant indicated this strain produced a developmental phenotype indistinguishable from the wild type with respect to fruiting body production and sporulation efficiency (100 ± 10 % of wild type). It is unlikely that the K48N substitution did not inactivate Pkn14 kinase activity, because it rendered Pkn14 incapable of autophosphorylation *in vitro* (Fig. 3A and data not shown). To confirm the mutant protein accumulated properly during development, we generated antibodies against the Pkn14 protein and performed anti-Pkn14 immunoblot analysis on protein lysates harvested from wild type, Δ*pkn14* and *pkn14*$_{K48N}$ mutants at 0, 12, 18, 24, and 36 hours of development. A band migrating at ~48 kDa could be detected in the wild type, but not Δ*pkn14* lysates, consistent with the Pkn14 predicted molecular mass of 45.4 kDa (Fig. 4C). Pkn14 was detected at highest levels in vegetative cells which

368 decreased 7.2-fold by 12 hours, remained constant at 18 and 24 hours, but was absent
369 by 36 hours. A similar pattern could be detected for Pkn14$_{K48N}$ (Fig. 4C). Thus, Pkn14
370 was expressed until at least the onset of aggregation, and disruption of auto-
371 phosphorylation did not significantly alter its accumulation pattern. To next examine
372 whether the *pkn14* mutants exhibited perturbed MrpC or FruA accumulation, we probed
373 the same samples with anti-MrpC or anti-FruA immunosera. We observed similar MrpC
374 and FruA accumulation in both the mutant *pkn14* strains compared to the wild type, with
375 the exception that FruA levels were very slightly delayed in the Δ*pkn14* mutant, likely as
376 a result of the delayed development observed in this strain (Fig. 4C).
377 Analysis of the of the Δ*pkn8* and *pkn8*$_{K116N}$ mutants revealed that they produced
378 developmental phenotypes indistinguishable from the wild type with respect to fruiting
379 body formation (Fig. 4A) and sporulation efficiency (97 ± 10 % and 98 ± 17 % of wild
380 type spores, respectively) (Fig. 4B); this phenotype was also in contrast to the early
381 developmental phenotype observed in the DZF1 background (Nariya & Inouye, 2005b).
382 Finally, to examine whether the Pkn14 and Pkn8 kinase activity was redundant, we
383 generated a double *pkn14*$_{K48N}$ *pkn8*$_{K116N}$ mutant. This mutant also displayed a wild type
384 developmental phenotype (Fig. 4A). The small reduction in sporulation efficiency
385 observed in this mutant during starvation (75 ± 12 %)- and glycerol (69 ± 8 %)-induced
386 sporulation was not considered statistically significantly different from wild type (Fig.
387 4B).
388 In summary, our genetic analyses suggested that under our laboratory developmental
389 conditions, Pkn8 has no obvious role in development and that the presence of Pkn14,
390 but not its kinase activity, is necessary to promote efficient developmental aggregation.

These data suggested that Pkn14-dependent phosphorylation of MrpC likely plays a role in controlling MrpC in response to perturbed conditions observed in the DZF1 background, which we are currently investigating. However, as the dramatic *mrpC*$_{AAAA}$ developmental phenotype suggested that the TTSS motif was essential for MrpC function, and little is known about how the activity of MrpC is intrinsically controlled, we set out to examine which of the activities attributed to MrpC were perturbed by this mutant.

Perturbation of the MrpC TTSS motif perturbs in vivo *MrpC activities*

As MrpC functions as a negative autoregulator (McLaughlin *et al.*, 2018) and the MrpC$_{AAAA}$ protein accumulated slightly earlier than wild type (Fig. 1D), we first addressed whether negative autoregulation was perturbed. The effect on autoregulation was analyzed with a reporter containing mCherry (mCh) under control of the *mrpC* promoter (P$_{mrpC}$-mCh) (McLaughlin *et al.*, 2018) which was integrated at the Mx8 phage *att* site in the wild type, *mrpC*$_{AAAA}$, and Δ*mrpC* backgrounds. The developmental phenotype observed in these strains bearing the reporter was indistinguishable from the parent strains (data not shown). To examine reporter activity, each strain was harvested at 0, 12, 18, 24, 30, 36, and 48 hours of development under submerged culture, and mCherry fluorescence was recorded and normalized to total protein. As we previously reported (McLaughlin *et al.*, 2018), mCherry signal in the wild type P$_{mrpC}$-mCh background gradually increased over 48 hours of development, and consistent with negative autoregulation, reporter activity increased at least 3.1-fold over wild type in the

414 Δ*mrpC* P_{mrpC}-mCh strain (Fig. 5A). In contrast, reporter activity in the *mrpC*$_{AAAA}$ P_{mrpC}-
415 mCh strain was only slightly higher with a maximum fold induction of 1.9-fold over wild
416 type at 36 hours (Fig. 5A). These results suggested that MrpC$_{AAAA}$ has a slight defect
417 in autoregulation which likely explains the elevated levels of MrpC$_{AAAA}$ observed in the
418 initial immunoblot analysis (Fig. 1).
419 During development, MrpC protein levels are also controlled by EspAC-dependent
420 proteolytic turnover (Schramm *et al.*, 2012). To examine whether the MrpC$_{\Delta N25}$ and
421 MrpC$_{AAAA}$ proteins were efficiently turned over, we examined the half-life of each protein
422 in chloramphenicol shutoff assays. For these experiments, the wild type, *mrpC*$_{AAAA}$, and
423 *mrpC*$_{\Delta N25}$ strains were induced to develop under submerged culture conditions for nine
424 hours, treated with chloramphenicol, and protein lysates harvested from cells after 0,
425 10, 20, 30, and 60 min were subject to anti-MrpC immunoblot. Consistent with previous
426 observations (Schramm *et al.*, 2012), we calculated an MrpC half-life of 24 $\pm$ 8 min.
427 However, MrpC$_{AAAA}$ and MrpC$_{\Delta N25}$ were not efficiently turned over ($t_{1/2}$ = 123 $\pm$ 14 and
428 244 $\pm$ 122 min, respectively)(Fig 5B). These results suggest that MrpC$_{\Delta N25}$ and
429 MrpC$_{AAAA}$ are not efficiently targeted for regulated proteolysis which likely also
430 contributes to the elevated levels observed *in vivo* for MrpC$_{AAAA}$ (Fig.1D) or MrpC$_{\Delta N25}$
431 (McLaughlin *et al.*, 2018).
432 MrpC is also a transcriptional activator and an important target is *fruA* (Ueki & Inouye,
433 2003). FruA is essential for induction of aggregation and sporulation (Ellehauge *et al.*,
434 1998, Ogawa *et al.*, 1996). We next examined the accumulation of FruA in the *att*::*mrpC*
435 and *mrpC*$_{AAAA}$ strains by anti-FruA immunoblot analysis of lysates prepared from cells
436 induced to develop under submerged culture conditions for 0, 12, 18, 24 and 36 hours.

437 In *att*::*mrpC* cells, FruA protein could be detected by 12 hours of development and
438 continued to accumulate to at least 36 hours (Fig. 5C). No FruA could be detected in the
439 Δ*mrpC* strain (Fig. 5C and data not shown). In contrast, production of FruA was
440 severely delayed and reduced in the *mrpC*$_{AAAA}$ lysates (Fig. 5C). Together, these results
441 suggested MrpC$_{AAAA}$ partially failed in repressing its own expression and was strongly
442 impaired in activating *fruA* expression. The failure to efficiently induce FruA likely
443 explained the failure to induce proper development observed in the *mrpC*$_{AAAA}$ mutant
444 (Fig. 1B).
445
446 *Perturbation of the MrpC TTSS motif reduces affinity for binding sites within the* mrpC
447 *and* fruA *promoters.*
448
449 To examine whether the MrpC$_{AAAA}$ protein was defective in binding to target promoters
450 *in vitro*, we used electrophoretic mobility shift assays to determine the relative affinity of
451 purified His$_6$-MrpC or His$_6$-MrpC$_{AAAA}$ for fluorescently labeled probes containing an
452 MrpC binding site (corresponding to -237 to -266 bp upstream from the *mrpC* start; aka
453 BS 5)(McLaughlin *et al.*, 2018). The bound and unbound fluorescent DNA probes were
454 resolved by gel electrophoresis and probes were detected by fluorescence imager. As
455 seen previously (McLaughlin *et al.*, 2018), 0.5-2 μM His$_6$-MrpC caused a progressively
456 increasing shift in the *mrpC* binding site probe. No shift was observed when excess
457 unlabeled probe was added indicating binding was specific (Fig 6A). In contrast, nearly
458 2 μM His$_6$-MrpC$_{AAAA}$ was required to detect a shift in the mobility of the probe,
459 suggesting an approximately 4-fold reduction in binding affinity (Fig. 6A).

To examine MrpC-binding to the *fruA* promoter, we first identified two putative MrpC binding sites situated at -366 to -395 (*fruA1*) and -341 to -370 bp (*fruA2*) from the *fruA* transcriptional start site, based on MrpC foot printing observed previously (Ueki & Inouye, 2003). When His_6-MrpC was incubated with the *fruA1* probe, we observed a shift in probe migration with at least 0.5 μM His_6-MrpC, whereas in the presence of His_6-$MrpC_{AAAA}$, an equivalent shift was observed at 2 μM (Fig. 6B). Similar results were observed if the *fruA2* probe was instead used (data not shown). These results indicated that His_6-$MrpC_{AAAA}$ affinity for both the *mrpC* and *fruA* probes was reduced approximately 4-fold. Thus, replacing the TTSS motif in MrpC appears to reduce efficient binding of MrpC to promoters from which MrpC represses (*mrpC*) or induces (*fruA*) transcription. Interestingly, the His_6-$MrpC_{\Delta N25}$ protein, which completely lacks the N-terminus binds with equal efficiency to *mrpC* (McLaughlin *et al.*, 2018) and *fruA* (data not shown) binding sites.

Most Crp/Fnr family transcriptional regulators are typically dimers in solution and ligand binding induces a conformational change that increases affinity for binding to target sequences on the DNA. However, *E. coli* Fnr activity is regulated by dimer-to-monomer transition upon oxidation of an Fe-S cluster coordinated by cysteine residues. Fnr also contains an amino-terminal extension, and three out of the four cysteines that coordinate the Fe-S cluster are located near the TTSS motif in MrpC (Fig. S4). To examine whether MrpC activity was likewise controlled by monomer-to-dimer transition, and whether the TTSS motif could be involved in this transition, we subjected 8 μM purified His_6-MrpC, His_6-$MrpC_{\Delta N25}$ or His_6-$MrpC_{AAAA}$ to gel filtration analysis on a Superdex^{TM} 200 10/300 GL column compared to molecular mass standards. For each

run, the absorbance at 280 nm (A_{280}) versus retention volume was recorded and 0.8 mL fractions were collected. Fractions corresponding to A_{280} peaks were examined by SDS-PAGE for MrpC. We observed peak His_6-MrpC, His_6-$MrpC_{\Delta N25}$, or His_6-$MrpC_{AAAA}$ in fractions corresponding to the A_{280} peaks at 15.3, 15.5, and 15.2 mL retention volumes, respectively (Fig. 6C). No MrpC was detected in the large peaks at ~10 mL retention volume which may have arisen due to light scattering. Analysis of the standard proteins indicated these retention volumes corresponded to molecular mass estimation of ~50-60 kDa, most consistent with dimer formation of MrpC; the calculated molecular masses of His_6-MrpC, His_6-$MrpC_{\Delta N25}$, and His_6-$MrpC_{AAAA}$ proteins is 30.6, 28.2 and 30.7 kDa, respectively. Thus, neither the deletion of the N-terminal region, nor substitution of the TTSS motif prevented formation of MrpC dimers *in vitro*. These results suggested the perturbation of the TTSS motif subtly altered the conformation of MrpC resulting in reduced affinity for target promoters.

DISCUSSION

MrpC is a Crp/Fnr transcriptional regulator that is essential for induction of aggregation and sporulation in the *M. xanthus* developmental program. A long-standing model suggested that the Pkn8/Pkn14 serine/threonine kinase cascade repressed MrpC activity by phosphorylating MrpC on threonine residues within its amino-terminal 25 residues (N25). Specifically, *in vitro* analyses showed that Pkn14 was sufficient to phosphorylate MrpC, and Pkn8 phosphorylates Pkn14, but not MrpC (Nariya & Inouye, 2005b). It was assumed that the threonine at position 21 and/or 22 was the phosphorylation target, because Pkn14 did not phosphorylate MrpC2, and thin layer

chromatography of acid-hydrolyzed MrpC~P indicated the phosphorylated residues corresponded to phospho-threonine. Phosphorylation was proposed to prevent proteolytic processing into MrpC2 (aka $MrpC_{\Delta N25}$), thought to be a more active isoform (Nariya & Inouye, 2006). This model was based on the observation that: 1) deletion of either *pkn8* or *pkn14* produced an early developmental phenotype, 2) 'MrpC2' was observed at higher levels in these strains, and 3) purified $MrpC_{\Delta N25}$ bound with higher affinity to target DNA sequences *in vitro*. However, we have recently demonstrated that the MrpC N25 is essential for activity *in vivo*, MrpC2 appears to be an artifact generated during cell lysis (McLaughlin *et al.*, 2018), and the observation that 'MrpC2' binds to target DNA sequences with higher affinity has not been reproduced (Robinson *et al.*, 2014, McLaughlin *et al.*, 2018). Therefore, we set out to elucidate the functional consequences of threonine phosphorylation in the MrpC amino-terminal region by the Pkn8/Pkn14 serine/threonine kinase cascade. Focusing first on a putative TTSS phosphorylation motif in N25, we demonstrated that substitution to AAAA inactivated MrpC *in vivo* (Figs. 1A, 2, and S2). However, as Pkn14 did not phosphorylate the TTSS directly *in vitro* (Fig. 3B), we instead conclude that the TTSS motif is necessary for appropriate recognition of MrpC by Pkn14 (Fig. 3B) and efficient binding to target promoters (Fig. 6). We also reveal *M. xanthus* strain-specific activation of the Pkn8/14 kinase cascade (Fig. 4). Finally, our data reveal MrpC has an important role in stabilizing *M. xanthus* development likely against micro-environmental and/or intrinsic noise (Figs. 2 and S2). We propose a revised model for control of MrpC activity that reconciles our data with previous observations; this model is presented in two parts below.

A revised model for Pkn8/Pkn14-dependent phosphorylation of MrpC

Our data revealed that Pkn8 and Pkn14 are not normally activated (i.e. auto-phosphorylated) under laboratory conditions in the wild type DZ2 *M. xanthus* strain, because kinase-dead versions of either (or both proteins) do not appreciably affect development (Fig. 4A and B). However, given the strong phenotype for both DZF1 *pkn14*$_{K48N}$ (Nariya & Inouye, 2008) and DZF1 Δ*pkn14* (Nariya & Inouye, 2005b) mutations (Fig. S3), we speculate that in the DZF1 background, Pkn14 is activated (Pkn14~P) resulting in a predominantly phosphorylated MrpC (MrpC~P) species, that represses MrpC activity. Therefore, relative to the parent, the DZF1 *pkn14* mutant displays an obvious early aggregation phenotype (Nariya & Inouye, 2005b)(Fig. S3), because MrpC activity is no longer repressed by phosphorylation. The stimulus activating Pkn14 (perhaps via Pkn8) may be related to envelope stress or altered energy stores, because the DZF1 background contains the partially defective *pilQ1* allele encoding a major outer membrane secretin necessary for efficient type IV-pili production (Wall *et al.*, 1999). *M. xanthus* type IV pili are necessary for social motility and are connected to production of surface polysaccharides (Yang *et al.*, 2010, Black *et al.*, 2017, Hu *et al.*, 2016), suggesting multiple energy intensive processes are likely altered in this background (Hu *et al.*, 2012).

Another puzzling observation was that although kinase-dead Pkn14 (Pkn14$_{K48N}$) did not display an obvious developmental phenotype in the DZ2 background, deletion of *pkn14* resulted in delayed development (Fig. 4A). These results suggest a specific role for

552 unphosphorylated Pkn14 in efficient induction of development. This role seems to be
553 largely independent of MrpC, because we do not observe drastic changes in MrpC or
554 FruA levels (targets of MrpC activity) in the Δ*pkn14* mutant (Fig. 4C). Pkn14 (along with
555 Pkn8) belongs to a large kinase / scaffold protein network (Nariya & Inouye, 2005c),
556 which includes at least two other kinases, Pkn9 and Pkn1, which appear to induce and
557 repress aggregation, respectively (Hanlon *et al.*, 1997, Munoz-Dorado *et al.*, 1991). We
558 suggest unphosphorylated Pkn14 affects aggregation indirectly through these proteins,
559 whereas when Pkn14 is stimulated to autophosphorylate, it instead represses
560 development by direct phosphorylation of MrpC. Thus, rather than functioning as a core
561 component in activation of MrpC, we suggest Pkn14 (and likely Pkn8) function to
562 modulate the developmental program in response to certain environmental conditions.
563 How could MrpC activity be repressed by phosphorylation? We did not detect *in vitro*
564 Pkn14-dependent phosphorylation of MrpC on threonine residues in the amino terminus
565 as previously proposed, but rather on adjacent serine threonine sites within the cNMP
566 domain (Ser_{55} Thr_{56}) and on four sites within the DNA binding domain (Fig. 3B). We
567 have not demonstrated the functionality of these residues, but the observation that
568 MrpC becomes phosphorylated in the DNA binding region is consistent with
569 observations that Pkn14-dependent phosphorylation of MrpC~P has been shown to
570 reduce binding to *mrpC* and *fruA* promoters *in vitro* (Nariya & Inouye, 2006). An
571 analogy can be drawn to the *Bradyrhizobium japonicum* (Bj) $FixK_2$ Crp/Fnr family
572 member, which regulates genes required for microoxic, anoxic, and symbiotic growth
573 during root nodule symbiosis with soybean plants (Nellen-Anthamatten *et al.*, 1998).
574 Bj$FixK_2$ binds target sequences in the absence of known ligand and modification of a

cysteine residue (Cys_{183}) located directly adjacent to the helix-turn-helix motif in the DNA binding domain reduces DNA affinity (Mesa *et al.*, 2009). Specifically, reactive oxygen species (ROS), which likely indicate conditions are not ideal for nodulation, convert the cysteine thiol to a bulky, negatively charged, sulfinic/sulfonic acid derivative which is proposed to sterically hinder the BjFixK$_2$-DNA interaction and repulse the phosphate backbone of the DNA (Bonnet *et al.*, 2013a). Intriguingly, one of the MrpC residues targeted by Pkn14, Thr_{191} (Fig. 3B), corresponds by sequence alignment and MrpC secondary structure prediction to BjFixK$_2$ Cys_{183} (Fig. S4A). Addition of a bulky negative charged phosphoryl group to Thr_{191} can be predicted to likewise hinder MrpC interactions with the DNA backbone.

The function of the additional MrpC residues observed to be phosphorylated by Pkn14 *in vitro* is unknown. While the observation that there are so many sites is surprising and certainly remains to be verified *in vivo*, multisite phosphorylation of transcription factors is a common phenomenon in eukaryotes contributing to integrated control of the intensity of transcription factor activation (Holmberg *et al.*, 2002). Consistently, *M. xanthus* encodes an unusually large number of eukaryotic-like serine/threonine protein kinases (Perez *et al.*, 2008) that are likely organized into integrated signaling networks that coordinate multiple physiological responses (Nariya & Inouye, 2005c) (Nariya & Inouye, 2002).

The role of the MrpC amino terminal extension

It was previously proposed that the MrpC amino-terminal extension (N25), which is not present in Crp homologs, must be removed for full MrpC activity. However, it is now clear that deletion of N25 in MrpC renders the protein inactive *in vivo* (McLaughlin *et al.*, 2018). An *mrpC*$_{\Delta N25}$ mutant is unable to: 1) aggregate or sporulate efficiently, 2) regulate *mrpC* expression by negative autoregulation (i.e. *mrpC* expression was not repressed), and 3) to induce FruA (McLaughlin *et al.*, 2018). Here, we additionally showed that MrpC$_{\Delta N25}$ was not subject to efficient proteolytic turnover (Fig. 5B). The recent observations that purified MrpC$_{\Delta N25}$ protein binds with equal affinity as full length MrpC to DNA target sequences *in vitro* (McLaughlin *et al.*, 2018, Robinson *et al.*, 2014), strongly suggests that the amino terminus is not required for DNA binding *per se*, but is required for additional contacts necessary to control transcription *in vivo*.

Our initial hypothesis at the start of this study was that phosphorylation of one or more residues in the TTSS motif modulates these proposed interactions. First, we demonstrated that complete replacement of TTSS with alanines produced similar, but slightly less extreme, results as the *mrpC*$_{\Delta N25}$ strain *in vivo*. The *mrpC*$_{AAAA}$ strain failed to aggregate and sporulate efficiently (Fig. 1B and C), displayed a reduced *mrpC* negative autoregulation (i.e. *mrpC* expression was inefficiently repressed) (Fig. 5A), induced FruA in efficiently (Fig. 5C) and was unable to effectively turnover MrpC$_{AAAA}$ (Fig. 5B). In contrast to MrpC$_{\Delta N25}$, however, purified MrpC$_{AAAA}$ displayed significantly reduced affinity for *mrpC* and *fruA* DNA binding sites (Fig. 6A and B). Circular dichroism analysis suggested that the MrpC$_{AAAA}$ mutation did not result in a drastically different secondary structure from the wild type (Fig. 3C). This observation reassured us that the reduction in DNA binding was not because the MrpC$_{AAAA}$ was partially unfolded and raised the

possibility that the TTSS to AAAA substitution may prevent the amino-terminus from assuming a configuration that stabilizes the DNA binding conformation of the protein. Finally, we did not detect Pkn14-dependent phosphorylation on the TTSS motif *in vitro* (Fig. 3B) and observed a general decrease in Pkn14-dependent phosphorylation on $MrpC_{AAAA}$, suggesting inefficient recognition of $MrpC_{AAAA}$ by Pkn14. We favor the interpretation that the entire amino terminus serves as a general protein interaction region, consistent with its intrinsic disorder prediction (data not shown). The TTSS motif in particular may act as a polar motif that allows stabilization of protein interactions, such as cooperative interactions with itself (Nariya & Inouye, 2006), contact with RNAP (Korner *et al.*, 2003), FruA (Korner *et al.*, 2003), or proteins that modulate the developmental program through MrpC, as we propose for Pkn14.

Many Crp/Fnr family members contain amino terminal extensions which are required for activity. For instance, the *E. coli* Fnr amino terminal extension contains three out of four of the cysteine residues which coordinate the Fe-S cluster that is necessary to sense anaerobic conditions (Spiro & Guest, 1990)(Fig. S4A). Intriguingly, MrpC structure predictions (Kelley *et al.*, 2015) model the TTSS motif at the end of an alpha helix that threads between the dimerization helix and the β-sheet scaffold and near to one of DNA binding helices in the helix-turn-helix motif (Fig. S5A). This arrangement has been seen in the crystal structure of *Mycobacterium tuberculosis* (Mt) Cmr (Ranganathan *et al.*, 2018), where the amino terminal extension (helix N1) is predicted to play a role in modulating DNA binding and/or dimerization perhaps in response to cellular signals (see Fig. S4A for alignments). Thus, interaction with other proteins, or unknown ligands, may reorient the amino-terminus. The TTSS motif may play a role in modulating this

643 reorientation. Our on-going efforts to solve the MrpC structure may illuminate how the
644 region could affect MrpC activity.
645 Interestingly, MrpC shares many architectural features with the Fnr-like branch of
646 transcriptional regulators that regulate gene transcription in response to anaerobic or
647 microoxic conditions. Like MrpC, BjFixK$_2$, as well as *E. coli* (Ec) Fnr, are regulated by
648 proteolytic turnover (Bonnet *et al.*, 2013b, Mettert & Kiley, 2005). BjFixK$_2$ contains
649 proteolytic sequence determinants in the extreme C-terminus of the protein which are
650 recognized and degraded by ClpAP$_1$ (Bonnet *et al.*, 2013b)(Fig. S4). In the case of
651 EcFnr, sequence determinants are found in the both the amino terminal 5-11 residues
652 and in the last two residues of the protein (residues 249 and 250)(Fig. S4), and
653 proteolytic turnover is dependent on ClpXP (Mettert & Kiley, 2005). We have shown
654 here that both MrpC$_{AAAA}$ and MrpC$_{\Delta N25}$ are not subject to proteolysis (Fig. 5B)
655 suggesting that the amino terminus may contain the sequence determinants for
656 proteolytic turnover. However, this interpretation is complicated by the observation that
657 EspA is highly reduced in the *mrpC*$_{AAAA}$ background (data not shown). EspA is an
658 integral component of the signaling system that induces proteolytic turnover of MrpC
659 (Mettert & Kiley, 2005), and *espA* expression is dependent on MrpC which binds to the
660 *espA* promoter *in vitro* (A. Schramm and P. Higgs, unpublished results).
661
662 *MrpC plays a role in stabilizing the developmental program*
663
664 A surprising finding from this study is that TTSS motif mutants bearing non-consecutive
665 T/S residues produce highly variable phenotypes ranging from wild type to early,

delayed, or retro development in different clones and in different biological replicates of the same clone (Figs. 2 and S2). These results reveal a previously unrecognized role for MrpC in maintaining developmental stability. It has been argued that developmental systems have evolved mechanisms to buffer against noisiness due to stochastic variation in numbers of regulatory molecules that must interact to promote progression through developmental pathways (Nijhout & Davidowitz, 2003, DeLaurier *et al.*, 2014). In the case of MrpC TTSS motif variants and *M. xanthus* development, this process most likely involves micro-environmental canalization, or buffering against phenotypic variation due to fine-scale environmental variation (such as slight differences in nutrient concentration or cell density between assays) and developmental noise (Nijhout & Davidowitz, 2003). Consistently, it has been recently observed that ultra-sensitive responses to nutrient concentration are mediated by MrpC (Hoang & Kroos, 2018). MrpC's role as an environmental capacitor is likely the result of its position as a hub in the genetic regulatory network. Multiple signaling systems feed into MrpC (Schramm *et al.*, 2012, Higgs *et al.*, 2008, Stein *et al.*, 2006, Nariya & Inouye, 2005a, Inouye & Nariya, 2008, Hoang & Kroos, 2018, Rajagopalan & Kroos, 2017), and MrpC directly and indirectly induces regulatory feedback loops (Kroos, 2007) (Hoang & Kroos, 2018). Furthermore, MrpC accumulation correlates with distinct cell fates: little or no MrpC is found in peripheral rods and highest accumulation in fruiting body cells (Lee *et al.*, 2012) and misaccumulation of MrpC can lead to inappropriate cell fate segregation (Cho & Zusman, 1999, Schramm *et al.*, 2012). Uncoordinated and/or inefficient MrpC interactions with target promoters or binding partners, or misaccumulation in inappropriate cell types, could result in stochastic phenotypes. Consistent with the

689 observation that MrpC may be phosphorylated on multiple sites, modeling approaches
690 have suggested that multisite phosphorylation is mechanism to filter noise (Aledo,
691 2018). We are currently examining whether MrpC is phosphorylated *in vivo* in response
692 to changing environmental conditions, whether the amino terminus is a general
693 interaction motif, and whether additional STPKs play a role in this process.
694

695 ## Experimental Procedures

696 *Bacterial growth and development conditions*

697 *E. coli* cells were grown at 37 °C on LB (0.1% tryptone, 0.5% yeast extract, 0.5% NaCl)
698 in agar plates (1.5%) or with shaking (220 rpm) in LB broth supplemented with 50 μg ml^{-1}
699 kanamycin, 100 μg ml^{-1} ampicillin, and/or 34 μg ml^{-1} chloramphenicol as needed.
700 Vegetative *M. xanthus* cells were grown at 32 °C on CYE (0.1% casitone, 0.5% yeast
701 extract, 10 mM MOPS-KOH, pH 7.6, 8 mM $MgSO_4$) 1.5% agar (Campos & Zusman,
702 1975) supplemented with 100 μg ml^{-1} kanamycin when necessary, or in CYE broth
703 (CYE without agar) with shaking at 220 rpm.
704 *M. xanthus* strains were induced to develop under submerged culture (Lee *et al.*, 2010)
705 unless otherwise indicated. Briefly, cells were grown overnight in CYE broth, diluted to
706 0.035 A_{550} in CYE and 0.5, 8, or 16 mL of cells was seeded into 24 well tissue culture
707 plates, or 60 mm or 150 mm petri dishes, respectively. Cells were grown into a
708 confluent layer at 32°C for 24 hours, then CYE was replaced with an equivalent volume
709 of MMC (10 mM MOPS pH 7.6, 4 mM $MgSO_4$, 2 mM $CaCl_2$) to induce development.
710 Cells were incubated undisturbed at 32°C, and pictures were recorded with a Leica
711 DMC 2900 stereo microscope.

For high-throughput, high resolution development imaging (Glaser & Higgs, 2019), cells were induced to develop by submerged culture as described above, except 0.15 mL cells were seeded into each well of a 96 well microtiter plate and incubated at 32 °C. After 24 hours of development, plates were transferred to a Tecan Infinite M200 plate reader (pre-warmed to 32 °C), and images were recorded from each well every 30 min from 24-72 hours post starvation using the plate reader cell confluence feature. Images were then assembled into movies in ImageJ (Schneider *et al.*, 2012) . For each movie, the time frame of developmental stages (onset of aggregation, initial aggregates, aggregates after consolidation/dissolution, mature aggregates, and darkened fruiting bodies) were manually recorded.

To determine the number of spores produced during development, cells were induced to develop by submerged culture in 24 well plates as described above. After 72 or 120 hours of starvation, cells from triplicate wells were harvested, pelleted at 17,000 x g for 5 min, supernatant was removed, and pellets stored at -20°C or used immediately. To kill non-spores, pellets were resuspended in 0.5 mL of water, heated at 50°C for 60 min, and sonicated three times for 30 sec (0.5 sec on 0.5 sec off) at 30% output on Branson Sonifier 250a equipped with a microtip. The remaining spherical and phase bright spores were enumerated on a Hawksley Helber bacteria hemocytometer.

The number of chemically-induced spores were determined as described previously (Holkenbrink *et al.*, 2014). Briefly, 25 mL cultures *M. xanthus* cells were grown at 32°C in CYE broth to an OD of ~ 0.3 A_{550}, 10 M sterile glycerol was added to a final concentration of 0.5 M and cultures were incubated at 32°C for 24 hours. The culture was pelleted and resuspended in 5 mL sterile water, and 3 x 0.5 mL were heated at

735 50°C for one hour and sonicated and counted as described above. Spore number was
736 reported as percent of starting cells, where an OD of 0.7 A_{550} corresponded to $4x10^8$
737 cells mL^{-1}
738
739 *Construction of plasmids and strains*
740 Plasmids used to construct *M. xanthus* strains (Table 1) were constructed using standard
741 restriction enzyme/ligation cloning techniques followed by transformation into *E. coli* strain
742 TOP10. For plasmids used to generate strains bearing in-frame deletions or point
743 mutations in the endogenous *M. xanthus* locus, gene fragments contained ~500 bp
744 fragments upstream and downstream from the desired deletion or point mutation and
745 were constructed by over-lap PCR as described previously in detail (Lee *et al.*, 2010),
746 and cloned into pBJ114 using the primers and enzymes listed in Table S2. For plasmids
747 used to express genes at the exogenous Mx8 phage attachment site, pFM18 (kan^R, Mx8
748 *attP*) was used. Plasmid insert fragments containing the native promoter and desired
749 mutated gene were initially constructed by overlap PCR or by direct PCR amplification
750 using the templates, primers, and enzymes listed in Table S2. For plasmids used to
751 express genes at the 1.38 kb *M. xanthus* genome integration site, P_{mrpC}-*mrpC* inserts
752 were cloned into pMR3679 (km^R, 1.38 kb recombination fragment), such that the vanillate
753 promoter was removed. Plasmid inserts were constructed as indicated in Table S2.
754 Strains bearing point mutations or in-frame deletions in the endogenous genetic locus
755 (Tables 1 and S1) were constructed using the strategy described in detail previously
756 (Lee *et al.*, 2010), Briefly, pBJ114 (*km^R*, *galK*) based plasmids were introduced into the
757 relevant *M. xanthus* strains by electroporation, and plasmid integration through

758 homologous recombination was selected by kanamycin-resistance. Plasmid loop-out
759 via a second homologous recombination event was screened by growth on 2-5%
760 galactose, and clones with the desired mutation were screened by PCR (in-frame
761 deletions) or PCR amplified and then sequenced (point mutations) (Lee *et al.*, 2010).
762 To generate strains bearing genes expressed from the Mx8 phage attachment site (*attB*),
763 pFM18 based plasmids (Tables 1 and S1) were electroporated into the relevant *M.*
764 *xanthus* strains and site-specific recombination into *attB* selected by kanamycin
765 resistance and screened for correct integration by PCR as described previously
766 (McLaughlin *et al.*, 2018). For strains bearing plasmid integrations at the 1.38kb
767 integration site, pMR3679-based plasmids were electroporated into the relevant *M.*
768 *xanthus* strains and homologous recombination into the 1.38 kb *M. xanthus* genome
769 region was selected by kanamycin resistance. Resulting colonies were screened by PCR
770 for correct integration as described previously (Garcia-Moreno *et al.*, 2009). For all
771 constructed strains, the developmental phenotypes of at least three independent clones
772 were assayed to confirm a true phenotype.
773 Protein expression plasmids were constructed using the templates, oligonucleotides,
774 and enzymes listed in Table S2.
775
776 *Immunoblot analysis*
777 To generate cell lysates for immunoblot analysis, *M. xanthus* was induced to develop in
778 150 mm petri dishes, as described above. At the indicated time points, cells were
779 harvested, pelleted at 4696 x g at 4°C, and cell pellets were either used immediately or
780 stored at -20°C. Cell pellets were resuspended in 0.5 mL of cold MMC, 0.5 mL of cold,

781 26% TCA was added, and tubes were incubated on ice for at least 15 minutes.
782 Precipitated proteins were pelleted at 4°C at 17,000 x g for 5 minutes, supernatant was
783 removed, the pellet was resuspended in 100% ice-cold acetone, centrifuged for 1
784 minute at room temperature, and repeated. After the second acetone wash, protein
785 pellets were resuspended in 100 µL of 100 mM Tris pH 8.0, 300 µL of clear LSB (62.5
786 mM Tris-HCl, pH 6.8, 10% (v/v) glycerol, 2% (w/v) SDS) was added, and samples were
787 heated at 94°C for 1 minute. Protein concentration in each sample was determined
788 using a BCA Protein Assay Kit (Pierce). Samples were diluted to 1 µg μL^{-1} in 2X LSB
789 (125 mM Tris-HCl, pH 6.8, 20% (v/v) glycerol, 4% (w/v) SDS, 10% (v/v) 2-
790 mercaptoethanol, 0.02% (w/v) bromophenol blue), heated at 99°C for 5 minutes, and
791 then stored at -20 °C. Protein samples were resolved by sodium dodecyl sulfate
792 polyacrylamide gel electrophoresis (SDS-PAGE) on a 13% (MrpC and FruA), or 9 %
793 (Pkn14) polyacrylamide gel, then transferred to a polyvinylidene fluoride (PVDF)
794 membrane (Millipore) in a semi-dry transfer apparatus (Hoefer TE77X). For Western
795 blots, membranes were either blocked for one hour at room temperature or overnight at
796 4°C in PBS (8 mM Na_2HPO_4, 2 mM KH_2PO_4 pH 7.4, 135 mM NaCl, 3.5 mM KCl)
797 supplemented with 0.1 % Tween and 5 % non-fat milk. Primary antibodies were used at
798 1:500 (anti-MrpC) (Garcia-Moreno *et al.*, 2009), 1:1000 (anti-FruA) (Lobedanz &
799 Sogaard-Andersen, 2003), or 1:500 (anti-Pkn14). Goat anti-rabbit, HRP-conjugated
800 secondary IgG secondary antibodies were used at 1:20 000 (Pierce).
801 Chemiluminescence (ECL Western Blotting Substrate, Pierce) and autoradiography film
802 (Andwin Scientific) were used for detection of immune complexes. For quantitation,

803 autoradiographs were scanned, and ImageQuant TL (GE Healthcare Life Sciences) was
804 used to quantify background-subtracted signal intensities.
805 Polyclonal rabbit anti-Pkn14 antibodies were generated by Eurogentec (Serain,
806 Belgium) using soluble purified Strep-Pkn14 protein. Purification was performed as
807 described below. Anti-Pkn14 antibodies were purified from serum against Step-Pkn14
808 protein as per (Jagadeesan *et al.*, 2009).
809
810 *Overexpression and purification of recombinant proteins*
811 Overexpression plasmids (Table 2) for recombinant His_6-tagged -MrpC, - $MrpC_{\Delta N25}$, -
812 $MrpC_{AAAA}$, or Trx-His_6, were freshly transformed into *E. coli* BL21(λDE3) cells and ~ 3
813 resulting colonies were grown overnight in 5 ml starter cultures, and then subcultured
814 (1:100) into 500 ml LB broth containing the appropriate antibiotic. His-tagged proteins
815 were induced in mid-log cells with 0.5 to 1 mM isopropyl 1-thio-β-D-galactopyranoside
816 (IPTG) for 3 hours at 25 or 37 °C. His-tagged proteins were then purified at 4°C either
817 by gravity flow (phosphotransfer and EMSA analyses) or FPLC (circular dichroism and
818 gel filtration analyses) using Ni-NTA resin (Qiagen) or 5-mL HisTrap column (GE
819 Healthcare), respectively. For purification of His_6-tagged proteins by gravity flow, cell
820 pellets were resuspended in 12 mL Lysis Buffer (50 mM HEPES-NaOH pH 7.4, 500 mM
821 NaCl, 20 mM imidizole) containing 1 mg mL^{-1} lysozyme and 1:100 protease inhibitor
822 cocktail (Sigma), and lysed by French press (18,000 psi, 3 times). Unlysed cells and/or
823 inclusion bodies were removed by centrifugation at 600 x g at 4°C for 30 min and
824 supernatant was applied to 0.5 mL Ni-NTA resin pre-equilibrated with lysis buffer,
825 washed with 5 column volumes (CV) Wash Buffer (50 mM HEPES pH 7.4, 500 mM

826 NaCl, 20 mM imidazole), and step-eluted with 3CV Elution Buffer (50 mM HEPES pH
827 7.4, 500 mM NaCl) containing 100 mM, 250 mM and then 500 mM imidazole. Elution
828 fractions containing peak amounts of purified protein were pooled, dialyzed in 900 ml
829 Dialysis Buffer 1 (50 mM HEPES pH 7.5, 250 mM NaCl, 1 mM dithiothreitol (DTT), 10%
830 (v/v) glycerol) for 1 hour at room temperature, then in 900 ml dialysis buffer 2 (Dialysis
831 Buffer 1 except 100mM NaCl and 20% glycerol) overnight at 4°C. Dialyzed proteins
832 were stored at -20°C. For FPLC purification of His-tagged proteins, induced cells were
833 resuspended in buffer B (20 mM Tris-HCl, 500 mM NaCl, 20 mM Imidazole pH 8.5) and
834 lysed by passing the cell suspension 3-5 times through an EmulsiFlex-C3 homogenizer
835 at 5,000-10,000 psi. Clarified lysate was loaded onto a 5-mL HisTrap column (GE
836 Healthcare) and weakly bound proteins were eluted off with a linear gradient from 20-
837 300 mM imidazole (buffer B to buffer C) followed by elution of His-tagged MrpC proteins
838 with buffer C (20 mM Tris-HCl, 100 mM NaCl, 900 mM Imidazole pH 8.9). Fractions
839 containing MrpC were pooled, concentrated, buffer-exchanged in buffer B, and stored at
840 4 ºC until further use.
841 Overexpression plasmids (Tables 1 and S2) for recombinant Step-tagged –Pkn14, or –
842 $Pkn14_{K48N}$, were freshly transformed and induced for overexpression as described
843 above except that the inducing agent was 0.06 µg mL^{-1} of anhydrotetracycline for 3
844 hours at 20°C. Cultures were then pelleted at 15,000 rpm for 15 minutes at 4°C, and
845 cell pellets were stored at -20°C until needed. For purification of Strep-tagged proteins,
846 cell pellets were resuspended in 30mL Buffer W (100 mM Tris pH 8.0, 150 mM NaCl, 1
847 mM EDTA) containing 1mg mL^{-1} lysozyme and 1:100 protease inhibitors, lysed by
848 French press, and cleared as described above. Cell supernatants were loaded onto

columns containing 0.8 ml Strep-Tactin resin (IBA) pre-equilibrated with Buffer W. Columns were washed with 5 CV Buffer W and Strep-tagged proteins were eluted with 4 CV Buffer E (100 mM Tris pH 8.0, 150 mM NaCl, 1 mM EDTA, 2.5 mM desthiobiotin); 0.8 mL fractions were collected, analyzed by SDS-PAGE, and elution fractions containing peak amounts of purified protein were pooled, dialyzed twice as described above except dialysis buffer contained 100 mM Tris pH 8.0, 150 mM NaCl, 1 mM DTT, 20% glycerol above, and stored at -20°C.

In vitro *kinase reactions and analysis*

Kinase reactions were carried out by incubating 6 µg of each purified kinase and substrate in buffer P (50 mM Tris pH 8.0, 2.4 mM ATP, 6 mM $MgCl_2$, 1 mM DTT) at 30°C for 30 minutes (typically in 30µL total volume), and quenched with an equal volume of 2 X LSB. 18 µL of each reaction was analyzed by SDS-13% PAGE. 1µL of phosphoprotein Molecular Weight Standards (Invitrogen) was included on the gel. Protein phosphorylation was visualized by incubating the gel in ProQ Diamond® phosphoprotein stain (Invitrogen) according to the manufacturer's instructions. Briefly, gels were incubated in 100 mL ProQ Diamond® fixing solution for at least 30 minutes, washed twice with water, then stained in ProQ Diamond® phosphoprotein stain for at least 75 minutes in the dark. Gels were destained in ProQ Diamond® destain solution three times for 30 minutes, then washed in water prior to imaging on a Typhoon FLA 7000 with an excitation wavelength of 532 nm and an R670 emission filter. Total protein was visualized by subsequently incubating rinsed gels in 60 mL Sypro Ruby stain (Invitrogen) overnight, followed by washes in Sypro Ruby wash solution for 30 minutes,

872 100 mL water two times for 5 minutes and then imaged at 532 nm excitation wavelength
873 and an O580 emission filter. Signal intensities were quantified using ImageQuant TL,
874 and background-subtracted phosphoprotein signal was normalized to background-
875 subtracted total protein signal, then plotted as the ratio of kinase active over kinase
876 dead reactions.
877
878 *Mass spectrometry*
879 For mass spectrometry analysis, Pkn14 kinase reactions with MrpC substrate were set
880 up as described above, except that 7.5 µg of each protein was used and reactions were
881 stopped by flash freeze in dry ice. Protein samples were then reduced with 5 mM
882 dithiothreitol (30 min at 65ºC) and alkylated with 20 mM iodoacetamide (30 min at room
883 temperature) in 50 mM ammonium bicarbonate, and digested with 1:50 dilution of
884 trypsin in 25 mM ammonium bicarbonate and 10% acetonitrile (overnight at 37ºC).
885 Peptides were dried and resuspended in a 2% trifluoroacetic acid and 65% acetonitrile
886 solution that was saturated with glutamic acid. Phosphopeptide enrichment was
887 performed using an AssayMAP Bravo automated liquid handler paired with TiO_2
888 cartridges (Agilent Technologies) according to manufacturer's instructions. Peptides
889 were eluted with a 5% ammonium hydroxide solution, dried, and resuspended in 0.1%
890 formic acid, 0.005% trifluoroacetic acid and 5% acetonitrile prior to LC/MS analysis.
891 Peptides were separated by UHPLC reverse phase chromatography using C18 columns
892 and an EASY-nLC system (Thermo) before introduction into an Orbitrap Fusion mass
893 spectrometer (Thermo). Settings for MS1 included a scan range of 375-1600 m/z at
894 240K resolution. For MS2 scans detected in the ion trap, peptides with +2 and +3

charges were fragmented by collision induced dissociation (CID) and peptides with charges +3 to +7 were fragmented by electron transfer dissociation (ETD). RAW files were searched with the Sequest algorithm within Proteome Discoverer (Thermo; ver 2.1) using 100 PPM and 0.6 Da tolerances for parent and fragment ions, respectively; fixed modification of carbamidomethylation of Cys; variable modifications of deamidation of Asn/Gln, oxidation of Met, and phosphorylation of Ser/Thr/Tyr; and up to 2 missed tryptic cleavages. Forward and reverse database searches were performed against a protein database for *Myxococcus xanthus* (downloaded from Uniprot on 2018-04-19; 8101 sequences). Results were imported into Scaffold (Proteome Software; ver 4.8) and a subset database was searched using X! Tandem. Peptide identifications were thresholded at a 1% false discovery rate (FDR).

Circular Dichroism

The CD-spectra of 56 µg ml^{-1} His_6-MrpC or His_6-$MrpC_{AAAA}$ in 20 mM Tris-HCl pH 8 and 100 mM NaCl were determined immediately after spinning the protein for 15 minutes at 20,000 x g with a Jasco 815 CD spectrometer with a 1 mm pathlength in the range λ = 190-260 nm. The spectra were collected in one pass with a bandwidth of 1 nm, scanning speed of 100 nm/min, and response time of 2 seconds at room temperature, following (Greenfield, 2006).

Analysis of mCherry fluorescence

Strains bearing the *mrpC* mCherry expression reporter (*attB*::P_{mrpC}-*mCherry*) were analyzed for mCherry fluorescence as described previously (McLaughlin *et al.*, 2018),

except fluorescence was recorded in a Tecan Infinite M200 plate reader at 582 nm excitation and 613 nm emission wavelengths. Briefly, strains were induced to develop under submerged culture in 24 well plates, triplicate wells were harvested, cells were dispersed, and triplicate 150 µL samples were analyzed for mCherry fluorescence intensity and normalized to total protein detected from remaining samples at each time point. Average data from three independent biological replicates was plotted.

Chloramphenicol shutoff assays

MrpC turnover was analyzed as described previously (Schramm *et al.*, 2012). Briefly, strains were induced to develop by submerged culture in 150 mm petri dishes, as described above. Chloramphenicol was added to a final concentration of 34 µg mL^{-1} to one petri dish per time point for each strain, and cells were harvested at 0, 10, 20, 30, or 60 minutes after addition of chloramphenicol, pelleted at 4 696 x g at 4°C, resuspended in 400 µL of 70°C 2X LSB, then heated at 99°C for 5 minutes. Equal proportions of samples were subject to anti-MrpC immunoblot as described above. ImageQuant TL was used to quantify background-subtracted signal intensities from duplicate replicates, and the signal intensity for each time point was normalized to that of t = 0 for each strain. The natural log of those values was plotted against time, and the slope (k) of the linear fit was used to calculate the half-life ($t_{1/2}$) of MrpC, using the equation $t_{1/2} = \ln(2)/-k$

Electrophoretic mobility shift assays

For electrophoretic mobility shift assays (EMSAs) were performed as described in detail, previously (McLaughlin *et al.*, 2018). Briefly, DNA probes consisted of three

annealed primers: a double Cy-5 labeled universal forward primer, an unlabeled forward primer that contained the protein binding site, and an unlabeled reverse primer that was complementary to both forward primers that were annealed in a thermocycler. The indicated concentrations of purified His_6-MrpC or His_6-$MrpC_{AAAA}$ were incubated with 50 nM labeled probe for 30 min at 20°C and then resolved on 10% polyacrylamide (37.5:1 acrylamide/bis-acrylamide gels in 0.5x TBE at 100V at 4°C. Gels were imaged with a Typhoon FLA 7000 [Pixel size: 25 μm, PMT: 500, Latitude: 4, Excitation wavelength: 635 nm, Emission filter: R670].

Gel filtration analyses

Analytical size-exclusion chromatography was carried out on a Superdex 200 10/300 GL column (GE Healthcare) equilibrated in 20 mM Tris-HCl, 500 mM NaCl, 20 mM imidazole pH 8.5 by an ÄKTA High Performance Liquid Chromatography (HPLC) apparatus. Eight μM His_6-MrpC, - $MrpC_{\Delta N25}$ or -MrpCAAAA proteins were applied with a flow rate of 0.5 ml min^{-1}. 0.8 mL fractions were collected, precipitated with trichloroacetic acid (TCA) and analyzed by SDS-PAGE. Molecular weight standards were used to calibrate the column: alcohol dehydrogenase (150 kDa), albumin (66 kDa), carbonic anhydrase (29 kDa), and myoglobin (17.6 kDa) had retention volumes of 13.0 mL, 14.67 mL 16.75 mL, and 17.35 mL respectively.

Acknowledgements

We gratefully acknowledge Xiaowei Mei for initial construction of *pkn8* and *pkn14* plasmids, Brian Nguyen for MrpC purification assistance, Petra Mann for technical

964 assistance, and Juan A. Arias Del Angel for stimulating discussions. This work was
965 funded by the National Science Foundation Career award IOS-1651921, Wayne State
966 startup funds, Wayne State Chemistry Biology Interface (CBI) fellowship (BF) and the
967 Max Planck Society (PH and VB).

968

969 ## Author Contributions

970 PIH conceived of the study. BF, VB, MM, SD, GB and PIH acquired and/or analyzed
971 data. PIH and BF wrote the manuscript.

972

973 ## Supporting Information

974

975 **Table S1**. Strains and plasmids used in supplementary data.

976 **Table S2**. Oligonucleotides and construction of plasmids used in this study.

977 **Figure S1**. Developmental phenotypes of MrpC TTSS motif mutants.

978 **Figure S2**. Insertion of P_{mrpC}-*mrpC* alleles at the 1.38kb *M. xanthus* genomic site does
979 not rescue loss of developmental robustness.

980 **Figure S3**. Developmental phenotype of Δ*pkn14* in the DZF1 versus DZ2 backgrounds.

981 **Figure S4.** Alignments of MrpC with Crp/Fnr homologs reveals functional residue
982 conservation.

983 **Figure S5.** Predicted MrpC tertiary structure.

984
985

REFERENCES

Aledo, J.C., (2018) Multisite phosphorylation provides a reliable mechanism for making decisions in noisy environments. *The FEBS journal* **285**: 3729-3737.

Benoff, B., H. Yang, C.L. Lawson, G. Parkinson, J. Liu, E. Blatter, Y.W. Ebright, H.M. Berman & R.H. Ebright, (2002) Structural basis of transcription activation: the CAP-alpha CTD-DNA complex. *Science* **297**: 1562-1566.

Black, W.P., L. Wang, X. Jing, R.C. Saldana, F. Li, B.E. Scharf, F.D. Schubot & Z. Yang, (2017) The type IV pilus assembly ATPase PilB functions as a signaling protein to regulate exopolysaccharide production in Myxococcus xanthus. *Scientific reports* **7**: 7263.

Bonnet, M., M. Kurz, S. Mesa, C. Briand, H. Hennecke & M.G. Grutter, (2013a) The structure of Bradyrhizobium japonicum transcription factor FixK2 unveils sites of DNA binding and oxidation. *The Journal of biological chemistry* **288**: 14238-14246.

Bonnet, M., M. Stegmann, Z. Maglica, E. Stiegeler, E. Weber-Ban, H. Hennecke & S. Mesa, (2013b) FixK(2), a key regulator in Bradyrhizobium japonicum, is a substrate for the protease ClpAP in vitro. *FEBS letters* **587**: 88-93.

Boynton, T.O., J.L. McMurry & L.J. Shimkets, (2013) Characterization of Myxococcus xanthus MazF and implications for a new point of regulation. *Molecular microbiology* **87**: 1267-1276.

Campos, J.M. & D.R. Zusman, (1975) Regulation of development in Myxococcus xanthus: effect of 3':5'-cyclic AMP, ADP, and nutrition. *Proceedings of the National Academy of Sciences of the United States of America* **72**: 518-522.

1009 Chin, K.H., Y.C. Lee, Z.L. Tu, C.H. Chen, Y.H. Tseng, J.M. Yang, R.P. Ryan, Y.
1010 McCarthy, J.M. Dow, A.H. Wang & S.H. Chou, (2010) The cAMP receptor-like
1011 protein CLP is a novel c-di-GMP receptor linking cell-cell signaling to virulence
1012 gene expression in Xanthomonas campestris. *Journal of molecular biology* **396**:
1013 646-662.
1014 Cho, K. & D.R. Zusman, (1999) Sporulation timing in Myxococcus xanthus is controlled
1015 by the espAB locus. *Molecular microbiology* **34**: 714-725.
1016 DeLaurier, A., T.R. Huycke, J.T. Nichols, M.E. Swartz, A. Larsen, C. Walker, J. Dowd,
1017 L. Pan, C.B. Moens & C.B. Kimmel, (2014) Role of mef2ca in developmental
1018 buffering of the zebrafish larval hyoid dermal skeleton. *Developmental biology*
1019 **385**: 189-199.
1020 Derouaux, A., S. Halici, H. Nothaft, T. Neutelings, G. Moutzourelis, J. Dusart, F.
1021 Titgemeyer & S. Rigali, (2004) Deletion of a cyclic AMP receptor protein
1022 homologue diminishes germination and affects morphological development of
1023 Streptomyces coelicolor. *Journal of bacteriology* **186**: 1893-1897.
1024 Dissmeyer, N. & A. Schnittger, (2011) Use of phospho-site substitutions to analyze the
1025 biological relevance of phosphorylation events in regulatory networks. *Methods in*
1026 *molecular biology* **779**: 93-138.
1027 Dworkin, M. & S.M. Gibson, (1964) A System for Studying Microbial Morphogenesis:
1028 Rapid Formation of Microcysts in Myxococcus Xanthus. *Science* **146**: 243-244.
1029 Ellehauge, E., M. Norregaard-Madsen & L. Sogaard-Andersen, (1998) The FruA signal
1030 transduction protein provides a checkpoint for the temporal co-ordination of

1031 intercellular signals in Myxococcus xanthus development. *Molecular microbiology*
1032 **30**: 807-817.
1033 Garcia-Moreno, D., J. Abellon-Ruiz, F. Garcia-Heras, F.J. Murillo, S. Padmanabhan &
1034 M. Elias-Arnanz, (2010) CdnL, a member of the large CarD-like family of
1035 bacterial proteins, is vital for Myxococcus xanthus and differs functionally from
1036 the global transcriptional regulator CarD. *Nucleic acids research* **38**: 4586-4598.
1037 Garcia-Moreno, D., M.C. Polanco, G. Navarro-Aviles, F.J. Murillo, S. Padmanabhan &
1038 M. Elias-Arnanz, (2009) A vitamin B12-based system for conditional expression
1039 reveals dksA to be an essential gene in Myxococcus xanthus. *Journal of*
1040 *bacteriology* **191**: 3108-3119.
1041 Glaser, M.M. & P.I. Higgs, (2019) Orphan Hybrid Histidine Protein Kinase SinK Acts as
1042 a Signal Integrator To Fine-Tune Multicellular Behavior in Myxococcus xanthus.
1043 *Journal of bacteriology* **201**.
1044 Greenfield, N.J., (2006) Using circular dichroism spectra to estimate protein secondary
1045 structure. *Nat Protoc* **1**: 2876-2890.
1046 Hanks, S.K., (2003) Genomic analysis of the eukaryotic protein kinase superfamily: a
1047 perspective. *Genome Biol* **4**: 111.
1048 Hanlon, W.A., M. Inouye & S. Inouye, (1997) Pkn9, a Ser/Thr protein kinase involved in
1049 the development of Myxococcus xanthus. *Molecular microbiology* **23**: 459-471.
1050 Higgs, P.I., S. Jagadeesan, P. Mann & D.R. Zusman, (2008) EspA, an orphan hybrid
1051 histidine protein kinase, regulates the timing of expression of key developmental
1052 proteins of Myxococcus xanthus. *Journal of bacteriology* **190**: 4416-4426.

1053 Hoang, Y. & L. Kroos, (2018) Ultrasensitive Response of Developing Myxococcus
1054 xanthus to the Addition of Nutrient Medium Correlates with the Level of MrpC.
1055 *Journal of bacteriology* **200**.
1056 Holkenbrink, C., E. Hoiczyk, J. Kahnt & P.I. Higgs, (2014) Synthesis and assembly of a
1057 novel glycan layer in Myxococcus xanthus spores. *The Journal of biological*
1058 *chemistry* **289**: 32364-32378.
1059 Holmberg, C.I., S.E. Tran, J.E. Eriksson & L. Sistonen, (2002) Multisite phosphorylation
1060 provides sophisticated regulation of transcription factors. *Trends Biochem Sci* **27**:
1061 619-627.
1062 Hu, W., M.L. Gibiansky, J. Wang, C. Wang, R. Lux, Y. Li, G.C. Wong & W. Shi, (2016)
1063 Interplay between type IV pili activity and exopolysaccharides secretion controls
1064 motility patterns in single cells of Myxococcus xanthus. *Scientific reports* **6**:
1065 17790.
1066 Hu, W., J. Wang, I. McHardy, R. Lux, Z. Yang, Y. Li & W. Shi, (2012) Effects of
1067 exopolysaccharide production on liquid vegetative growth, stress survival, and
1068 stationary phase recovery in Myxococcus xanthus. *Journal of microbiology* **50**:
1069 241-248.
1070 Inouye, S. & H. Nariya, (2008) Dual regulation with Ser/Thr kinase cascade and a
1071 His/Asp TCS in Myxococcus xanthus. *Advances in experimental medicine and*
1072 *biology* **631**: 111-121.
1073 Jagadeesan, S., P. Mann, C.W. Schink & P.I. Higgs, (2009) A novel "four-component"
1074 two-component signal transduction mechanism regulates developmental

progression in Myxococcus xanthus. *The Journal of biological chemistry* **284**: 21435-21445.

Julien, B., A.D. Kaiser & A. Garza, (2000) Spatial control of cell differentiation in Myxococcus xanthus. *Proceedings of the National Academy of Sciences of the United States of America* **97**: 9098-9103.

Kanack, K.J., L.J. Runyen-Janecky, E.P. Ferrell, S.J. Suh & S.E. West, (2006) Characterization of DNA-binding specificity and analysis of binding sites of the Pseudomonas aeruginosa global regulator, Vfr, a homologue of the Escherichia coli cAMP receptor protein. *Microbiology* **152**: 3485-3496.

Kelley, L.A., S. Mezulis, C.M. Yates, M.N. Wass & M.J. Sternberg, (2015) The Phyre2 web portal for protein modeling, prediction and analysis. *Nat Protoc* **10**: 845-858.

Kiley, P.J. & H. Beinert, (1998) Oxygen sensing by the global regulator, FNR: the role of the iron-sulfur cluster. *FEMS microbiology reviews* **22**: 341-352.

Korner, H., H.J. Sofia & W.G. Zumft, (2003) Phylogeny of the bacterial superfamily of Crp-Fnr transcription regulators: exploiting the metabolic spectrum by controlling alternative gene programs. *FEMS microbiology reviews* **27**: 559-592.

Kroos, L., (2007) The Bacillus and Myxococcus developmental networks and their transcriptional regulators. *Annual review of genetics* **41**: 13-39.

Lazazzera, B.A., D.M. Bates & P.J. Kiley, (1993) The activity of the Escherichia coli transcription factor FNR is regulated by a change in oligomeric state. *Genes & development* **7**: 1993-2005.

Lee, B., C. Holkenbrink, A. Treuner-Lange & P.I. Higgs, (2012) Myxococcus xanthus developmental cell fate production: heterogeneous accumulation of

1098 developmental regulatory proteins and reexamination of the role of MazF in
1099 developmental lysis. *Journal of bacteriology* **194**: 3058-3068.
1100 Lee, B., A. Schramm, S. Jagadeesan & P.I. Higgs, (2010) Two-component systems and
1101 regulation of developmental progression in Myxococcus xanthus. *Methods in*
1102 *enzymology* **471**: 253-278.
1103 Lee, J.S., B. Son, P. Viswanathan, P.M. Luethy & L. Kroos, (2011) Combinatorial
1104 regulation of fmgD by MrpC2 and FruA during Myxococcus xanthus
1105 development. *Journal of bacteriology* **193**: 1681-1689.
1106 Letunic, I. & P. Bork, (2018) 20 years of the SMART protein domain annotation
1107 resource. *Nucleic acids research* **46**: D493-D496.
1108 Lobedanz, S. & L. Sogaard-Andersen, (2003) Identification of the C-signal, a contact-
1109 dependent morphogen coordinating multiple developmental responses in
1110 Myxococcus xanthus. *Genes & development* **17**: 2151-2161.
1111 McLaughlin, M., V. Bhardwaj, B.E. Feeley & P.I. Higgs, (2018) MrpC, a CRP/Fnr
1112 homolog, functions as a negative autoregulator during the Myxococcus xanthus
1113 multicellular developmental program. *Molecular microbiology*.
1114 McNicholas, S., E. Potterton, K.S. Wilson & M.E. Noble, (2011) Presenting your
1115 structures: the CCP4mg molecular-graphics software. *Acta Crystallogr D Biol*
1116 *Crystallogr* **67**: 386-394.
1117 Mesa, S., L. Reutimann, H.M. Fischer & H. Hennecke, (2009) Posttranslational control
1118 of transcription factor FixK2, a key regulator for the Bradyrhizobium japonicum-
1119 soybean symbiosis. *Proceedings of the National Academy of Sciences of the*
1120 *United States of America* **106**: 21860-21865.

1121 Mettert, E.L. & P.J. Kiley, (2005) ClpXP-dependent proteolysis of FNR upon loss of its
1122 O2-sensing [4Fe-4S] cluster. *Journal of molecular biology* **354**: 220-232.
1123 Mittal, S. & L. Kroos, (2009a) A combination of unusual transcription factors binds
1124 cooperatively to control Myxococcus xanthus developmental gene expression.
1125 *Proceedings of the National Academy of Sciences of the United States of*
1126 *America* **106**: 1965-1970.
1127 Mittal, S. & L. Kroos, (2009b) Combinatorial regulation by a novel arrangement of FruA
1128 and MrpC2 transcription factors during Myxococcus xanthus development.
1129 *Journal of bacteriology* **191**: 2753-2763.
1130 Muller, F.D., A. Treuner-Lange, J. Heider, S.M. Huntley & P.I. Higgs, (2010) Global
1131 transcriptome analysis of spore formation in Myxococcus xanthus reveals a locus
1132 necessary for cell differentiation. *BMC genomics* **11**: 264.
1133 Munoz-Dorado, J., S. Inouye & M. Inouye, (1991) A gene encoding a protein
1134 serine/threonine kinase is required for normal development of M. xanthus, a
1135 gram-negative bacterium. *Cell* **67**: 995-1006.
1136 Munoz-Dorado, J., F.J. Marcos-Torres, E. Garcia-Bravo, A. Moraleda-Munoz & J.
1137 Perez, (2016) Myxobacteria: Moving, Killing, Feeding, and Surviving Together.
1138 *Frontiers in microbiology* **7**: 781.
1139 Nariya, H. & M. Inouye, (2008) MazF, an mRNA interferase, mediates programmed cell
1140 death during multicellular Myxococcus development. *Cell* **132**: 55-66.
1141 Nariya, H. & S. Inouye, (2002) Activation of 6-phosphofructokinase via phosphorylation
1142 by Pkn4, a protein Ser/Thr kinase of Myxococcus xanthus. *Molecular*
1143 *microbiology* **46**: 1353-1366.

Nariya, H. & S. Inouye, (2005a) Factors that modulate the Pkn4 kinase cascade in Myxococcus xanthus. *Journal of molecular microbiology and biotechnology* **9**: 147-153.

Nariya, H. & S. Inouye, (2005b) Identification of a protein Ser/Thr kinase cascade that regulates essential transcriptional activators in Myxococcus xanthus development. *Molecular microbiology* **58**: 367-379.

Nariya, H. & S. Inouye, (2005c) Modulating factors for the Pkn4 kinase cascade in regulating 6-phosphofructokinase in Myxococcus xanthus. *Molecular microbiology* **56**: 1314-1328.

Nariya, H. & S. Inouye, (2006) A protein Ser/Thr kinase cascade negatively regulates the DNA-binding activity of MrpC, a smaller form of which may be necessary for the Myxococcus xanthus development. *Molecular microbiology* **60**: 1205-1217.

Nellen-Anthamatten, D., P. Rossi, O. Preisig, I. Kullik, M. Babst, H.M. Fischer & H. Hennecke, (1998) Bradyrhizobium japonicum FixK2, a crucial distributor in the FixLJ-dependent regulatory cascade for control of genes inducible by low oxygen levels. *Journal of bacteriology* **180**: 5251-5255.

Nijhout, H.F. & G. Davidowitz, (2003) Developmental Perspectives on Phenotypic Variation, Canalization and Fluctuating Asymmetry. In: Developmetnal Instability: Causes and Consequences. M. Polak (ed). Oxford Univeristy Press, pp.

O'Connor, K.A. & D.R. Zusman, (1991) Behavior of peripheral rods and their role in the life cycle of Myxococcus xanthus. *Journal of bacteriology* **173**: 3342-3355.

1165 Ogawa, M., S. Fujitani, X. Mao, S. Inouye & T. Komano, (1996) FruA, a putative
1166 transcription factor essential for the development of Myxococcus xanthus.
1167 *Molecular microbiology* **22**: 757-767.
1168 Perez, J., A. Castaneda-Garcia, H. Jenke-Kodama, R. Muller & J. Munoz-Dorado,
1169 (2008) Eukaryotic-like protein kinases in the prokaryotes and the myxobacterial
1170 kinome. *Proceedings of the National Academy of Sciences of the United States*
1171 *of America* **105**: 15950-15955.
1172 Rajagopalan, R. & L. Kroos, (2014) Nutrient-regulated proteolysis of MrpC halts
1173 expression of genes important for commitment to sporulation during Myxococcus
1174 xanthus development. *Journal of bacteriology* **196**: 2736-2747.
1175 Rajagopalan, R. & L. Kroos, (2017) The dev Operon Regulates the Timing of
1176 Sporulation during Myxococcus xanthus Development. *Journal of bacteriology*
1177 **199**.
1178 Ranganathan, S., J. Cheung, M. Cassidy, C. Ginter, J.D. Pata & K.A. McDonough,
1179 (2018) Novel structural features drive DNA binding properties of Cmr, a CRP
1180 family protein in TB complex mycobacteria. *Nucleic acids research* **46**: 403-420.
1181 Robinson, M., B. Son, D. Kroos & L. Kroos, (2014) Transcription factor MrpC binds to
1182 promoter regions of hundreds of developmentally-regulated genes in
1183 Myxococcus xanthus. *BMC genomics* **15**: 1123.
1184 Rosenbluh, A., R. Nir, E. Sahar & E. Rosenberg, (1989) Cell-density-dependent lysis
1185 and sporulation of Myxococcus xanthus in agarose microbeads. *Journal of*
1186 *bacteriology* **171**: 4923-4929.

1187 Saha, A., J. Mukhopadhyay, A.B. Datta & P. Parrack, (2015) Revisiting the mechanism
1188 of activation of cyclic AMP receptor protein (CRP) by cAMP in Escherichia coli:
1189 lessons from a subunit-crosslinked form of CRP. *FEBS letters* **589**: 358-363.
1190 Saha, S., P. Patra, O. Igoshin & L. Kroos, (2019) Systematic analysis of the
1191 Myxococcus xanthus developmental gene regulatory network supports
1192 posttranslational regulation of FruA by C-signaling. *Molecular microbiology*.
1193 Schneider, C.A., W.S. Rasband & K.W. Eliceiri, (2012) NIH Image to ImageJ: 25 years
1194 of image analysis. *Nat Methods* **9**: 671-675.
1195 Schramm, A., B. Lee & P.I. Higgs, (2012) Intra- and interprotein phosphorylation
1196 between two-hybrid histidine kinases controls Myxococcus xanthus
1197 developmental progression. *The Journal of biological chemistry* **287**: 25060-
1198 25072.
1199 Sievers, F., A. Wilm, D. Dineen, T.J. Gibson, K. Karplus, W. Li, R. Lopez, H. McWilliam,
1200 M. Remmert, J. Soding, J.D. Thompson & D.G. Higgins, (2011) Fast, scalable
1201 generation of high-quality protein multiple sequence alignments using Clustal
1202 Omega. *Mol Syst Biol* **7**: 539.
1203 Soberon-Chavez, G., L.D. Alcaraz, E. Morales, G.Y. Ponce-Soto & L. Servin-Gonzalez,
1204 (2017) The Transcriptional Regulators of the CRP Family Regulate Different
1205 Essential Bacterial Functions and Can Be Inherited Vertically and Horizontally.
1206 *Frontiers in microbiology* **8**: 959.
1207 Sogaard-Andersen, L. & D. Kaiser, (1996) C factor, a cell-surface-associated
1208 intercellular signaling protein, stimulates the cytoplasmic Frz signal transduction

system in Myxococcus xanthus. *Proceedings of the National Academy of Sciences of the United States of America* **93**: 2675-2679.

Son, B., Y. Liu & L. Kroos, (2011) Combinatorial regulation by MrpC2 and FruA involves three sites in the fmgE promoter region during Myxococcus xanthus development. *Journal of bacteriology* **193**: 2756-2766.

Spiro, S. & J.R. Guest, (1990) FNR and its role in oxygen-regulated gene expression in Escherichia coli. *FEMS microbiology reviews* **6**: 399-428.

Stein, E.A., K. Cho, P.I. Higgs & D.R. Zusman, (2006) Two Ser/Thr protein kinases essential for efficient aggregation and spore morphogenesis in Myxococcus xanthus. *Molecular microbiology* **60**: 1414-1431.

Sun, H. & W. Shi, (2001) Genetic studies of mrp, a locus essential for cellular aggregation and sporulation of Myxococcus xanthus. *Journal of bacteriology* **183**: 4786-4795.

Ueki, T. & S. Inouye, (2003) Identification of an activator protein required for the induction of fruA, a gene essential for fruiting body development in Myxococcus xanthus. *Proceedings of the National Academy of Sciences of the United States of America* **100**: 8782-8787.

Viswanathan, P., T. Ueki, S. Inouye & L. Kroos, (2007) Combinatorial regulation of genes essential for Myxococcus xanthus development involves a response regulator and a LysR-type regulator. *Proceedings of the National Academy of Sciences of the United States of America* **104**: 7969-7974.

Wall, D., P.E. Kolenbrander & D. Kaiser, (1999) The Myxococcus xanthus pilQ (sglA) gene encodes a secretin homolog required for type IV pilus biogenesis, social motility, and development. *Journal of bacteriology* **181**: 24-33.

Wireman, J.W. & M. Dworkin, (1977) Developmentally induced autolysis during fruiting body formation by Myxococcus xanthus. *Journal of bacteriology* **129**: 798-802.

Yang, Z., R. Lux, W. Hu, C. Hu & W. Shi, (2010) PilA localization affects extracellular polysaccharide production and fruiting body formation in Myxococcus xanthus. *Molecular microbiology* **76**: 1500-1513.

1240 **Table 1. Strains and plasmids used in this work.**

***M. xanthus* strains**		
Strain	**Genotype**	**Source**
DZ2	Wild type	(Campos & Zusman, 1975)
PH1025	DZ2 Δ*mrpC*	(Lee *et al.*, 2012)
PH1108	DZ2 $mrpC_{\Delta N25}$	(McLaughlin *et al.*, 2018)
PH1139	DZ2 $mrpC_{AAAA}$	This study
PH1118	PH1025 *attB*::P_{mrpC}-*mrpC*, Km^R	(McLaughlin *et al.*, 2018)
PH1530	PH1025 *attB*::P_{mrpC}-$mrpC_{AAAA}$, Km^R	This study
PH1531	PH1025 *attB*::P_{mrpC}-$mrpC_{TAAA}$, Km^R	This study
PH1532	PH1025 *attB*::P_{mrpC}-$mrpC_{AAAS}$, Km^R	This study
PH1547	PH1025 *attB*::P_{mrpC}-$mrpC_{TASA}$, Km^R	This study
PH1533	PH1025 *attB*::P_{mrpC}-$mrpC_{ETSS}$, Km^R	This study
PH1132	DZ2 Δ*pkn14*	This study
PH1133	DZ2 $pkn14_{K48N}$	This study
PH1347	DZ2 Δ*pkn8*	This study
PH1548	DZ2 $pkn8_{K116N}$	This study
PH1549	PH1133 $pkn8_{K116N}$	This study
PH1100	DZ2 *attB*::P_{mrpC}-*mCherry*, Km^R	(McLaughlin *et al.*, 2018)
PH1104	PH1025 *attB*::P_{mrpC}-*mCherry*, Km^R	(McLaughlin *et al.*, 2018)
PH1306	PH1139 *attB*::P_{mrpC}-*mCherry*, Km^R	This study
***E. coli* strains**		
Strain	**Genotype**	**Source**
TOP10	F^- *endA1 recA1 galE15 galK16 nupG rpsL* Δ*lacX74* Φ80*lacZ*ΔM15 *araD139* Δ(ara, leu)7697 *mcrA* Δ(*mrr-hsdRMS-mcrBC*) λ^-	Invitrogen
BL21 λDE3	F^- *ompT gal dcm lon* $hsdS_B$ (r_B^- m_B^-)λ (DE3 [*lacI lacUV5*-T7 gene 1 *ind1 sam7 nin5*])	Novagen
Plasmid	**Genotype**	**Source**
Mutagenesis plasmids		
pBJ114	Suicide plasmid with Km^R and galK	(Julien *et al.*, 2000)
pVG129	pBJ114 $mrpC_{AAAA}$	This study
pFM18	Mx8 phage *attP* integration plasmid	(Muller *et al.*, 2010)
pBEF010	pFM18 P_{mrpC}-$mrpC_{AAAA}$	This study
pBEF007	pFM18 P_{mrpC}-$mrpC_{TAAA}$	This study
pBEF011	pFM18 P_{mrpC}-$mrpC_{AAAS}$	This study
pBEF015	pFM18 P_{mrpC}-$mrpC_{TASA}$	This study
pBEF006	pFM18 P_{mrpC}-$mrpC_{ETSS}$	This study
pXM001	pBJ114 Δ*pkn14*	This study

pVG125	pBJ114 *pkn14*$_{K48N}$	This study
pXM002	pBJ114 Δ*pkn8*	This study
pXM003	pBJ114 *pkn8*$_{K116N}$	This study
pPTM014	Mx8 *attP*, P$_{mrpC}$-*mCherry*	(McLaughlin *et al.*, 2018)
Overexpression plasmids		
pET28a+	T7 promotor, His$_6$ tag (N-terminal), *Km*^{R}	Novagen
pPH158	pET28a+ *mrpC*, Km^R	(Lee *et al.*, 2012)
pPH167	pET28a+ *mrpC*$_{ΔN25}$, Km^R	(McLaughlin *et al.*, 2018)
pVG131	pET28a+ *mrpC*$_{AAAA}$, Km^R	This study
pASK-IBA15+	*tet* promoter, *Strep* tag II (N-terminal), *Ap*^{R}	IBA Lifesciences
pPH166	pASK-IBA15+ *pkn14*	This study
pVG130	pASK-IBA15+ *pkn14*$_{K48N}$	This study
pET32a+	T7 promoter, Trx, His$_6$ tag, *Ap*^{R}	Novagen

1243 # FIGURES

1244

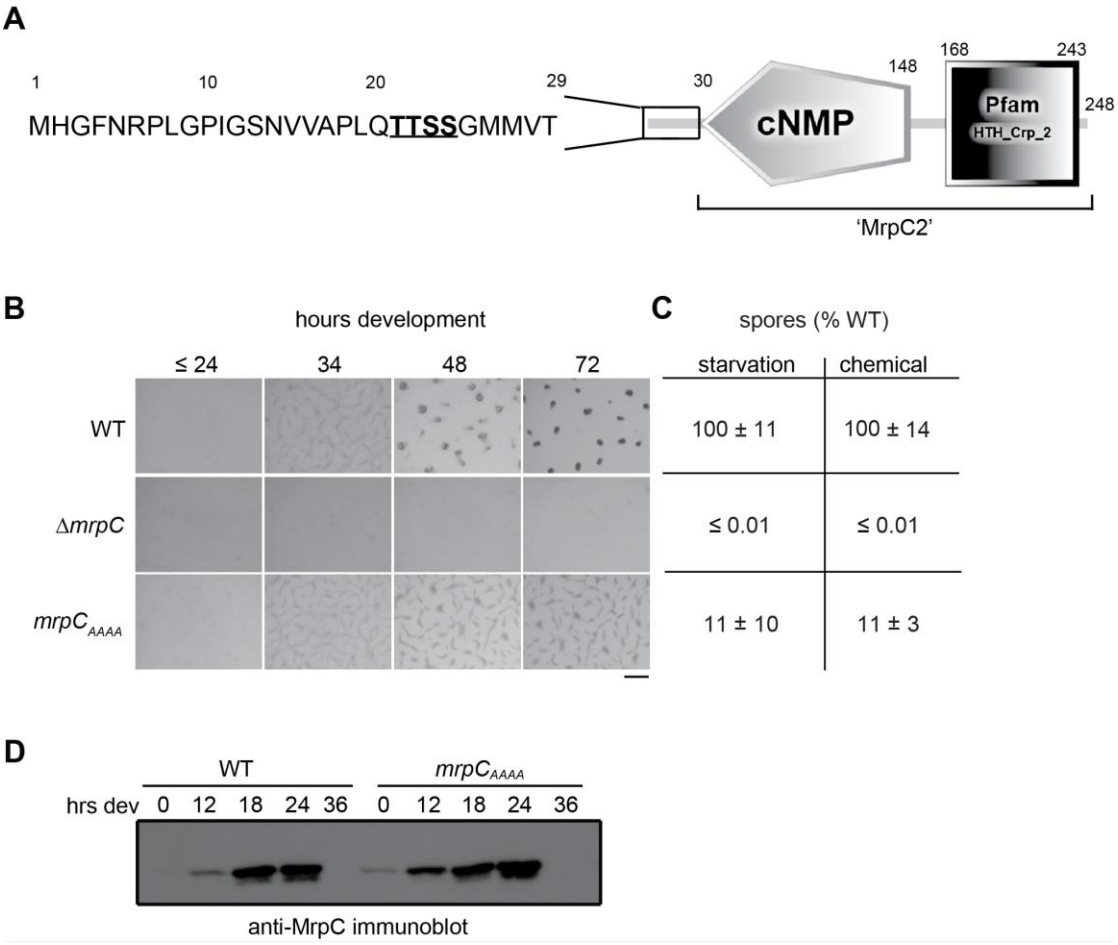

1245

1246

1247 Figure 1. A TTSS motif within the N-terminus of MrpC is necessary for function. A.

1248 Domain architecture of MrpC depicted by SMART analysis (Letunic & Bork, 2018)

1249 showing the predicted cyclic nucleotide monophosphate binding (cNMP) and DNA

1250 binding domains (Pfam HTH_Crp_2). The sequence of the N-terminal 29 residues is

1251 shown with the TTSS motif underlined and in bold. Residue numbers are depicted

1252 above. "MrpC2" (aka $MrpC_{N25}$) is a truncated MrpC that lacks the N-terminal 25

1253 residues. B. Developmental phenotypes of wildtype (wt: DZ2), Δ*mrpC* (PH1025), and

1254 *mrpC*$_{AAAA}$ (PH1139) strains induced to develop under submerged culture and recorded
1255 at the indicated hours post-starvation. Bar: 0.5 mm C. Percent of wild type heat and
1256 sonication resistant spores harvested from cells developed for 72 hours under
1257 submerged culture (starvation) or after 24 hours of chemical induction with 0.5 M
1258 glycerol (chemical). Values are the average and associated standard deviations from
1259 three independent biological replicates. D. Anti-MrpC immunoblot analysis of protein
1260 lysates harvested from wild type (WT: DZ2) or *mrpC*$_{AAAA}$ (PH1139) cells developing
1261 under submerged culture for the indicated hours.
1262

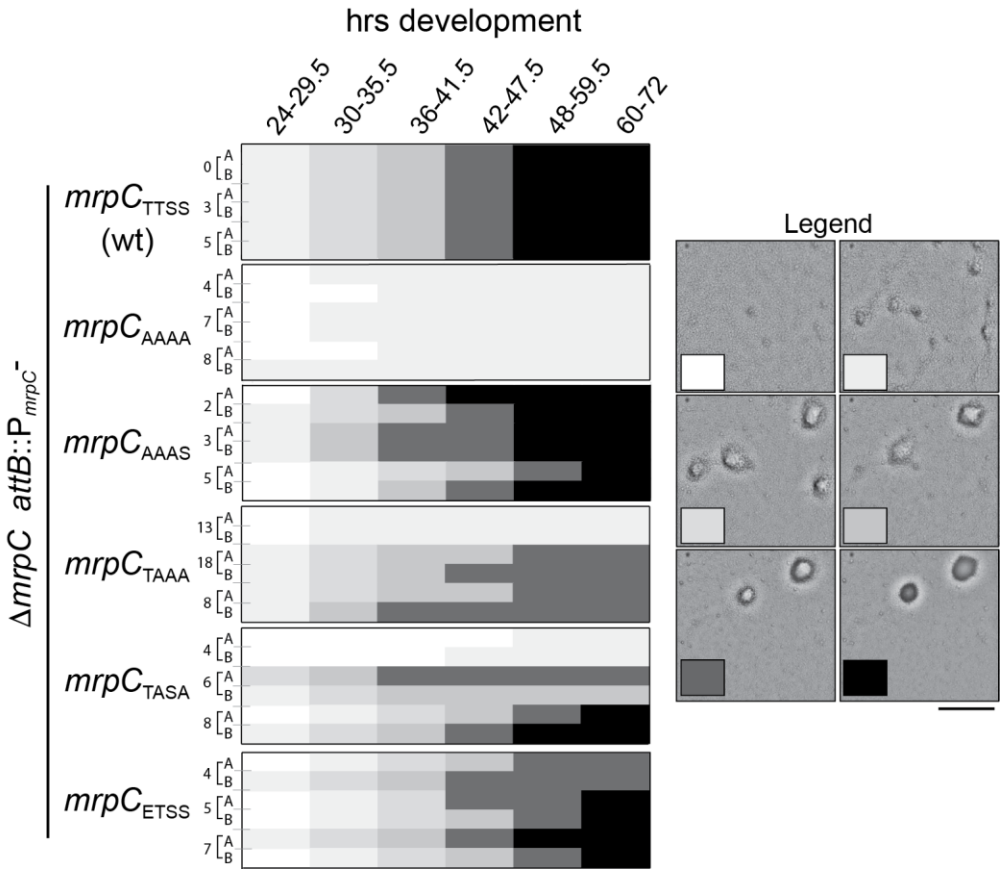

Figure 2. Lack of consecutive intact MrpC TTSS motif residues leads to loss of developmental robustness. Inter- and intra-clone variability in the developmental phenotypes of *mrpC*$_{TTSS}$ (wild type)(PH1118), *mrpC*$_{AAAA}$ (PH1530), *mrpC*$_{AAAS}$ (PH1532), *mrpC*$_{TAAA}$ (PH1531), *mrpC*$_{TASA}$ (PH1547), and *mrpC*$_{ETSS}$ (PH1533) genes integrated at the *attB* site in the Δ*mrpC* background. The heat maps shown indicate the variability in the timing and extent of completion of fruiting body formation during development under submerged culture conditions in 96 well plates in the indicated ranges of developmental times. Replicates are indicated by letters (A,B), and independent clones are represented by clone number. The shade of box corresponds to the extent of

1274 development as indicated by representative pictures in the legend (see text for details).

1275 Bar: 250 µm.

1276

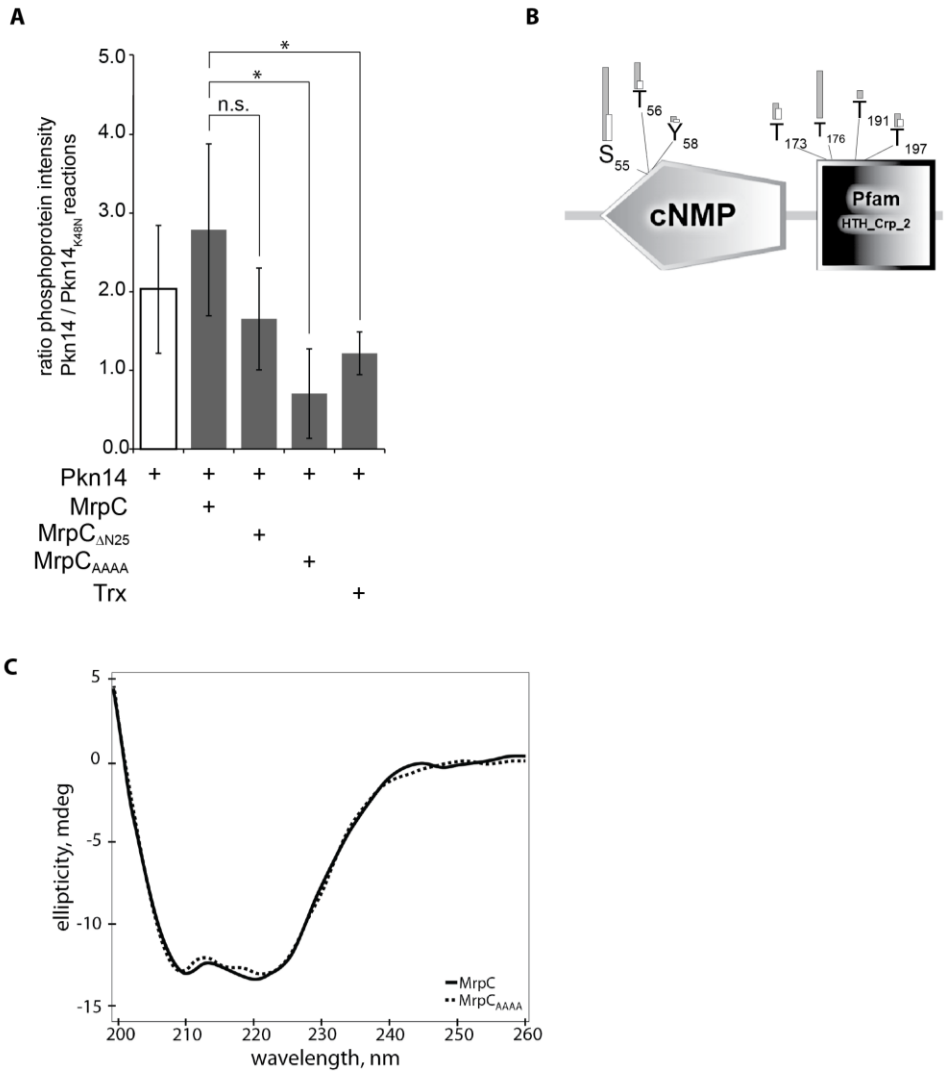

Figure 3. Pkn14 does not phosphorylate MrpC on the TTSS motif *in vitro*. A. Specific phosphoprotein stain intensities from Strep-Pkn14 autophosphorylation (white bar) or from Pkn14-dependent phosphorylation of His_6-MrpC, His_6-$MrpC_{\Delta N25}$, His_6-$MrpC_{AAAA}$, or the non-specific protein Trx-His_6, as indicated (grey bars). For each reaction, Strep-Pkn14 or –$Pkn14_{K48N}$ were incubated in kinase buffer and indicated substrate. Reactions were resolved by protein gel electrophoresis, and phosphorylated proteins were detected by phosphoprotein stain, and then by total protein stain. Phosphoprotein

signal intensities were first normalized to total protein and then normalized to phosphoprotein signal intensities from the kinase dead $Pkn14_{K48N}$ reactions. Data points are the averages and associated standard deviations from three independent replicates. *, *p*-value ≤ 0.05 as determined by Student's t-test; n.s., not significant. B. Pkn14-dependent phosphorylated residues on MrpC detected by mass spectrometry. *In vitro* kinase reactions containing Pkn14 or $Pkn14_{K48N}$ and MrpC or $MrpC_{AAAA}$ were trypsin digested and TiO_2-enriched phosphopeptides were subject to MS/MS analysis. Peptides are shown which meet stringent cutoff criteria (minimum 5 peptides detected, 0.1% FDR). Phosphorylation counts on MrpC (grey bars) or $MrpC_{AAAA}$ (white bars) residues are shown. No phosphorylation counts were detected in the respective $Pkn14_{K48N}$ reactions. The MrpC domain architecture from SMART analysis is depicted (Letunic & Bork, 2018). C. Circular dichroism analysis of His-MrpC (blue trace) and His-$MrpC_{AAAA}$ (red trace). Measurements were performed under ionic conditions similar to those used in our *in vitro* assays.

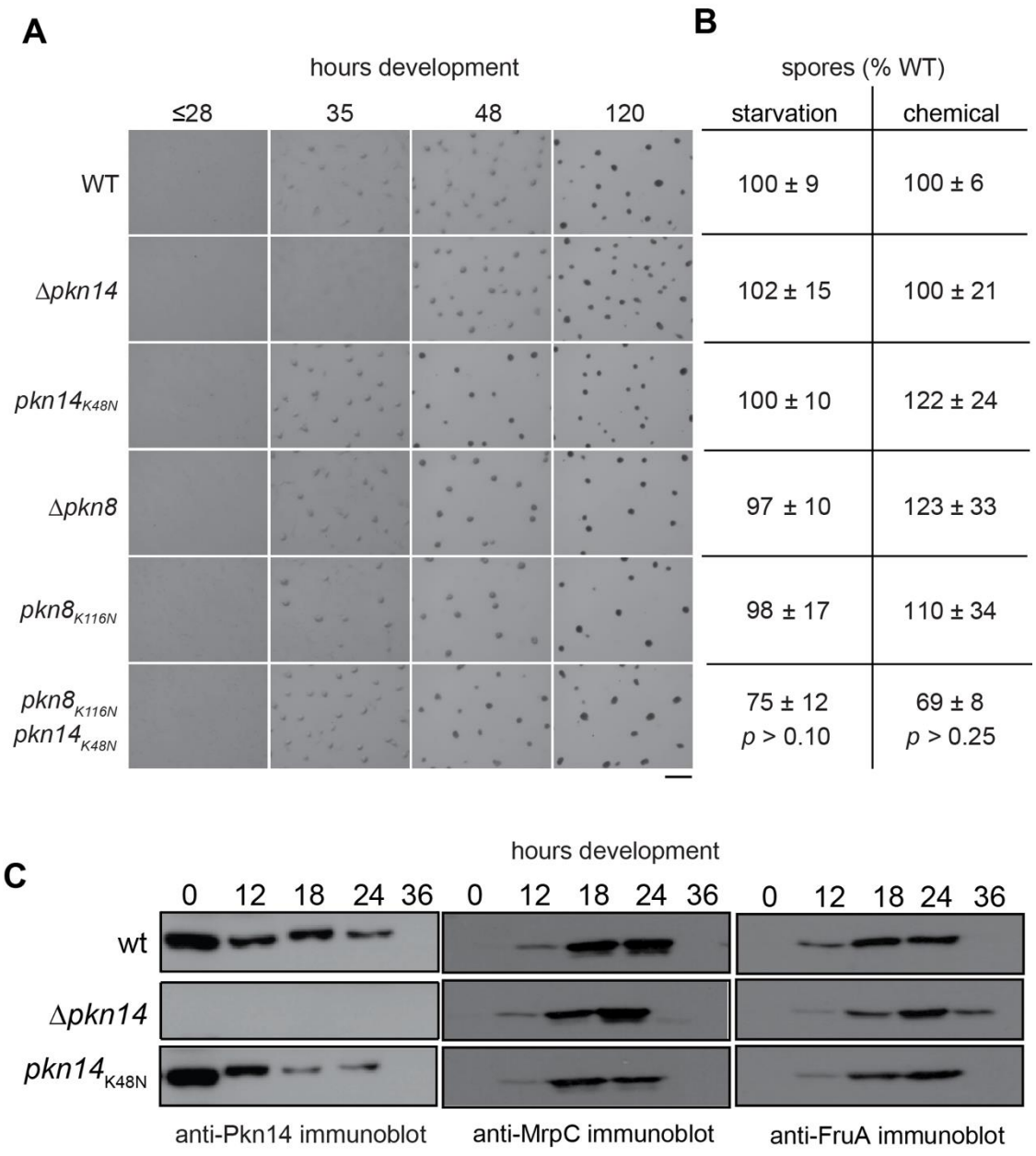

Figure 4. Pkn8/Pkn14 do not repress development in the *M. xanthus* DZ2 strain background. A. Developmental phenotypes of wild type DZ2, Δ*pkn14* (PH1132), $pkn14_{K48N}$ (PH1133), Δ*pkn8* (PH1347), $pkn8_{K116N}$ (PH1548) and double point mutant $pkn14_{K48N}\,pkn8_{K116N}$ (PH1549) strains were induced to develop by submerged culture conditions and images were recorded at the indicated hours of development. Bar: 0.5mm. B. Sporulation efficiencies from starvation-induced development (left) and

chemical induced development (right). The number of heat and sonication resistant spores harvested after 120 hrs development (left) or 24 hours of induction (right) and reported as a percent of wildtype, respectively. Values are the average and associated standard deviations from three independent biological replicates. *p*-value was determined by chi-square analysis. C. Pkn14, MrpC, and FruA accumulation profiles in wild type (DZ2), Δ*pkn14* (PH1132), $pkn14_{K48N}$ (PH1133) or cells. 10 μg lysates generated from cells induced to develop under submerged culture for the indicated hours post-starvation were subject to anti-Pkn14, -MrpC, or -FruA immunoblot, as indicated.

1323

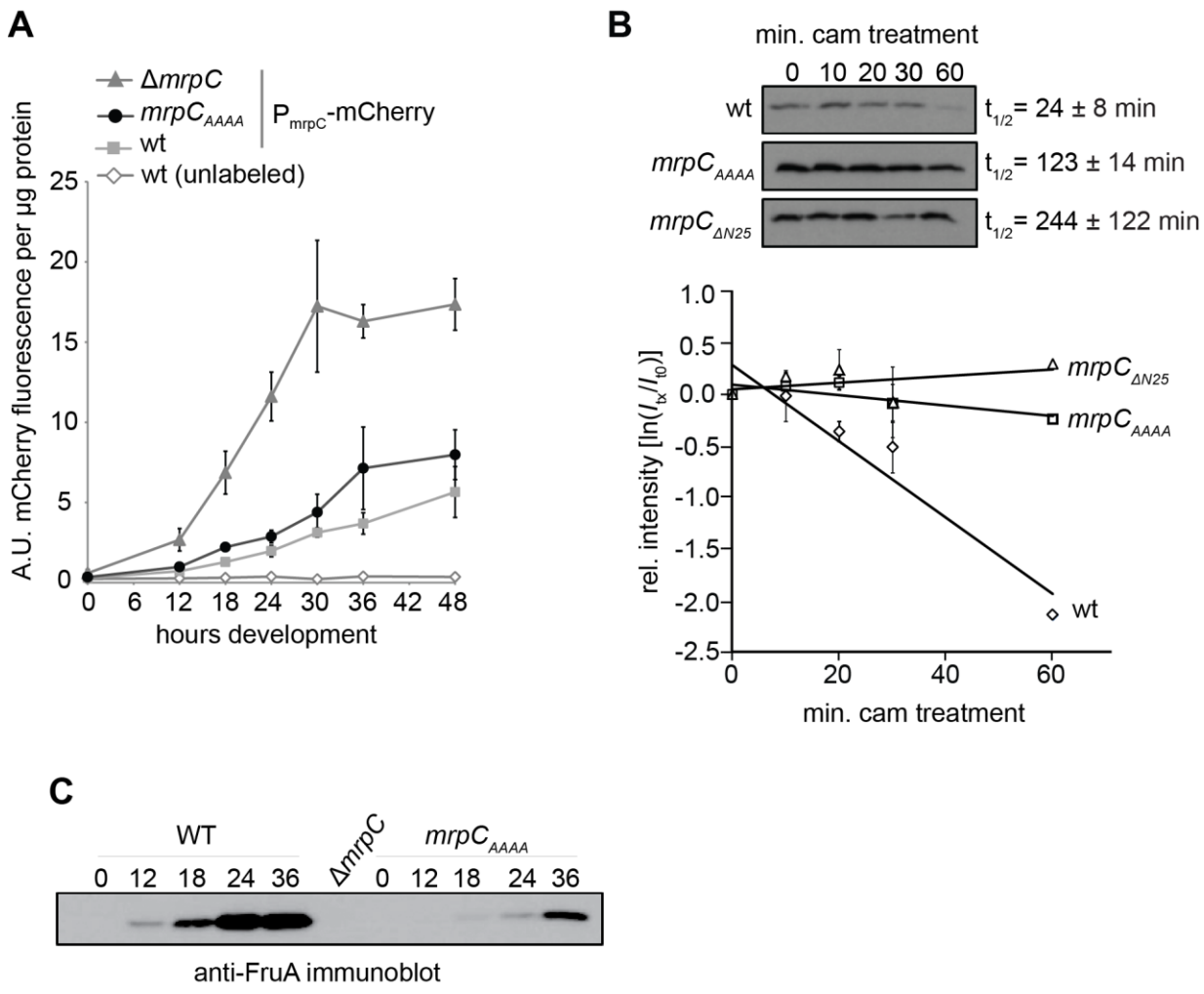

1324

1325 Figure 5. MrpC$_{AAAA}$ is perturbed in *mrpC* negative autoregulation, MrpC turnover, and

1326 FruA induction. A. Expression of a P$_{mrpC}$-*mCherry* reporter in wild type (PH1100),

1327 Δ*mrpC* (PH1104), and *mrpC$_{AAAA}$* (PH1306) backgrounds. Cells were induced to

1328 develop under submerged culture conditions and harvested at the indicated times.

1329 mCherry fluorescence was recorded as arbitrary units (A. U.) and then normalized to

1330 total protein. Values are the average and associated standard deviations from three

1331 independent biological replicates. Wild type unlabeled (DZ2) cells lack the reporter. B.

1332 MrpC turnover assay. Wild type (wt; DZ2), *mrpC*$_{AAAA}$ (PH1139), or *mrpC*$_{\Delta N25}$ (PH1108)

strains were induced to develop under submerged culture conditions for 9 hours and treated with 34 ug ml^{-1} chloramphenicol (cam) for the indicated times. Equal cell amounts of each sample were subjected to anti-MrpC immunoblot (upper panels). MrpC half-lives were calculated from two independent biological replicates where the MrpC band intensity for each time point was normalized to the intensity at T=0 of the respective strain and, and the natural log of the normalized intensities was plotted versus min of chloramphenicol treatment (lower graph). The slope of the linear fit of the data was used to calculate the MrpC half-life ($t_{1/2}$) in each strain for each replicate, and those values were averaged. Values plotted are the average and associated standard deviation for each time point from the two replicates. C. Anti-FruA immunoblot analysis of protein lysates harvested from Δ*mrpC attB*::P_{mrpC}-$mrpC_{TTSS}$ (WT: PH1118) or DZ2 $mrpC_{AAAA}$ (PH1139) strains developing under submerged culture conditions for the indicated hours. The Δ*mrpC* lysate (PH1025) was prepared from cells at 24 hours of development.

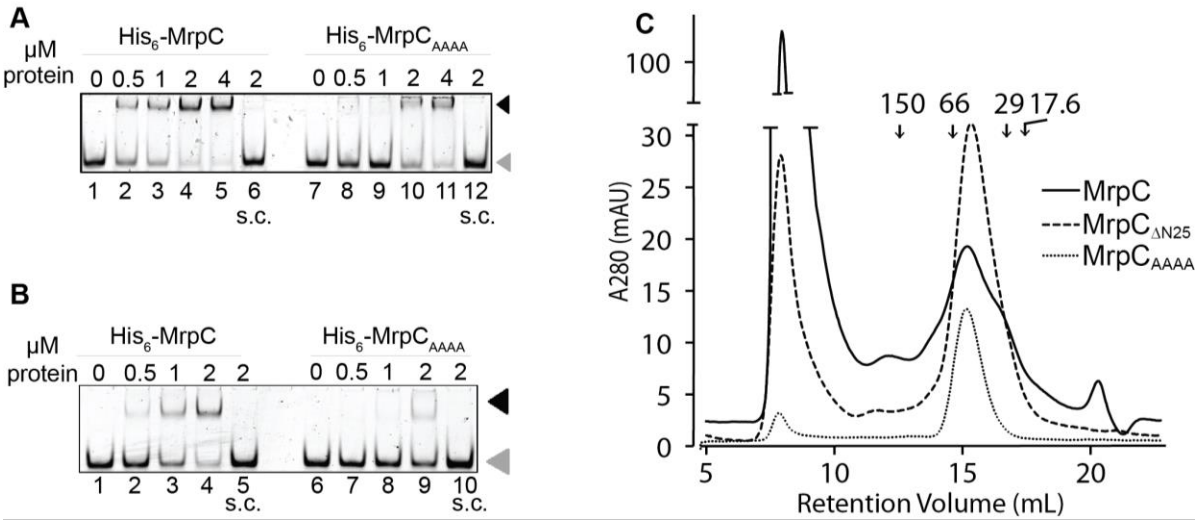

1348

1349 Figure 6. MrpC$_{AAAA}$ does not efficiently bind to *mrpC* or *fruA* promoter binding sites. A.

1350 Electrophoretic mobility shift assays (EMSAs) of His$_6$-MrpC or His$_6$-MrpC$_{AAAA}$ using

1351 *mrpC* promoter binding site 5. Increasing concentration (0-4 micromolar, as labeled) of

1352 His$_6$-MrpC (lanes 1-6) or His$_6$-MrpC$_{AAAA}$ (lanes 7-12) was incubated with 50 nM of

1353 fluorescently labeled probe. B. EMSA as in A. using *fruA1* promoter binding site.

1354 Increasing concentration (0-2 micromolar, as labeled) of His$_6$-MrpC (lanes 1-5) or His$_6$-

1355 MrpC$_{AAAA}$ (lanes 6-10) was incubated with 50 nM of fluorescently labeled probe. Lanes 6

1356 and 12 (A), or 5 and 10 (B) additionally contain 2.7 μM of the respective unlabeled

1357 probe (s.c., specific chase). Black arrowhead, protein + DNA complex; gray arrowhead,

1358 unbound DNA probe. C. MrpC$_{AAAA}$ and MrpC$_{\Delta N25}$ retain dimerization capability in

1359 solution. Analytical size-exclusion chromatography on a Superdex^{TM} 200 10/300 GL

1360 column using 4 nmol (8 μM x 500 μl) His$_6$-MrpC (red), His$_6$- MrpC$_{\Delta N25}$ (blue) or His$_6$-

1361 MrpC$_{AAAA}$ (black). Retention volumes of alcohol dehydrogenase (150 kDa), albumin (66

1362 kDa), carbonic anhydrase (29 kDa), and myoglobin (17.6 kDa) are depicted. Peak

1363 MrpC, MrpC$_{\Delta N25}$, or MrpC$_{AAAA}$ fractions corresponded to peaks at retention volumes of

1364 15.3, 15.5, and 15.2 mL, respectively, consistent with MrpC dimers (~50~60 kDa).